J. Fluid Mech. (1995), *vol.* 286, *pp.* 67–101

Free-surface flow due to impulsive motion of a submerged circular cylinder

By PEDER A. TYVAND[1] AND TOUVIA MILOH[2]

[1] Department of Agricultural Engineering, Agricultural University of Norway, 1432 Ås, Norway

[2] Department of Fluid Mechanics and Heat Transfer, Tel Aviv University, Ramat Aviv, Tel Aviv 69 978, Israel

(Received 4 January 1994 and in revised form 27 September 1994)

The impulsively starting motion of a circular cylinder submerged horizontally below a free surface is studied analytically using a small-time expansion. The series expansion is taken as far as necessary to include the leading gravitational effects for two cases: constant velocity and constant acceleration, both commencing from rest. The hydrodynamic force on the cylinder and the surface elevation are calculated and expressed in terms of bipolar coordinates. Comparisons are also made with earlier theoretical and experimental work. The theory is valid for arbitrary value of submergence depth to cylinder radius.

1. Introduction

The interaction of a circular cylinder with a free surface is a well-established subject in hydrodynamics. The first paper was written by Dean (1948) on linear wave diffraction due to a restrained cylinder. Dean's results were confirmed by Ursell (1950), who also studied the corresponding radiation problem. At the same time, Havelock (1949*a*, *b*) introduced the type of problem that we are proposing to study here: the transient free-surface response due to a cylinder that is suddenly set into forced motion at time zero.

The early papers by Havelock (1949*a*, *b*) treated the impulsively starting motion of a cylinder, with constant velocity and constant acceleration, respectively. Based on linear theory, the full free-surface time evolution was studied. Havelock's work was extended into the nonlinear regime by Tuck (1965). In the present paper we will carry further the analytical approach to this problem. However, in contrast to these early papers, we are not interested here in the long-time evolution predicted by linear theory, but in the short-time successive triggering of nonlinear effects. These can be studied in terms of a small-time expansion of the full nonlinear initial/boundary value problem (e.g. Peregrine 1972; Greenhow & Lin 1983; Vinje 1994).

The full initial/boundary value problem for an impulsively started submerged cylinder in an inviscid fluid has been studied by Haussling & Coleman (1979), Telste (1987), Greenhow (1988, 1993) and Terent'ev (1991). Ananthakrishnan & Yeung (1994) have recently studied the start of an oscillatory motion, both for viscous and inviscid flow. However, all these results are solely numerical, and cannot give accurate predictions of the forces at small times. Small-time expansions for the slamming force acting on a rigid sphere, during both vertical and oblique water-entries, have been calculated by Miloh (1991*a*, *b*). Greenhow & Lin (1983) have investigated the present problem experimentally, but for vertical motion only. In the present paper the initial

velocity is allowed to make an arbitrary oblique angle with the undisturbed free surface. We take into account the leading-order effects of gravity (arbitrary Froude number), and the ratio of the cylinder radius to the submergence depth is also arbitrary. The small-cylinder limit of the present problem is investigated in an accompanying paper (Tyvand & Miloh 1995).

In this paper we put emphasis on a consistent treatment of the important geometric nonlinearity due to the fact that the cylinder is displaced away from its initial position, at any finite time since its start. This geometric nonlinearity has recently been investigated by Wu (1993), in the context of the radiation problem for a submerged circular cylinder with a linearized free-surface condition.

2. General mathematical problem

We consider a solid circular cylinder of radius $\mathfrak{R}$ submerged in an inviscid fluid of infinite depth. At negative times ($t < 0$) everything is at rest, and the cylinder centre is located at a distance D below the free surface of the fluid. Cartesian coordinates x and y are introduced. The gravitational acceleration is denoted by g, and the y-axis is directed upwards. The x-axis lies at the undisturbed free surface (see figure 1). The surface elevation is denoted by $\eta = \eta(x, t)$. We introduce a unit velocity W, which will be specified later. The unit of length is the initial submergence depth D. The important dimensionless parameter in the present formulation is the Froude number defined by

$$Fr = \frac{W}{(gD)^{1/2}}. \tag{2.1}$$

We also introduce units of dimensionless time D/W and pressure ρW^2, where ρ is the fluid density. The dimensionless cylinder radius is chosen as

$$\epsilon = \mathfrak{R}/D. \tag{2.2}$$

The primary choice for W is the initial velocity, but in order to avoid exclusion of an important special case, we leave this definition open for the time being.

The forced motion starts impulsively from rest at time zero. According to Kelvin's circulation theorem (Batchelor 1967, p. 273), the flow is irrotational. The continuity equation for an incompressible fluid then implies that the fluid motion is governed by Laplace's equation,

$$\nabla^2 \Phi = 0, \tag{2.3}$$

where $\Phi(x, y, t)$ is the dimensionless velocity potential. The dimensionless boundary conditions are

$$|\nabla \Phi| \to 0, \quad x^2 + y^2 \to \infty, \tag{2.4}$$

$$\frac{\partial \eta}{\partial t} + \frac{\partial \Phi}{\partial x}\frac{\partial \eta}{\partial x} = \frac{\partial \Phi}{\partial y}, \quad y = \eta(x, t), \tag{2.5}$$

$$\frac{\partial \Phi}{\partial t} + \tfrac{1}{2}|\nabla \Phi|^2 + Fr^{-2}\eta = 0, \quad y = \eta(x, t), \tag{2.6}$$

$$(\boldsymbol{r} - \boldsymbol{R}) \cdot (\nabla \Phi - \dot{\boldsymbol{R}}) = 0, \quad |\boldsymbol{r} - \boldsymbol{R}| = \epsilon. \tag{2.7}$$

The dot superscript denotes time differentiation. We have introduced here the following notation for the position vector of a fluid particle:

$$\boldsymbol{r} = x\boldsymbol{i} + y\boldsymbol{j}, \tag{2.8}$$

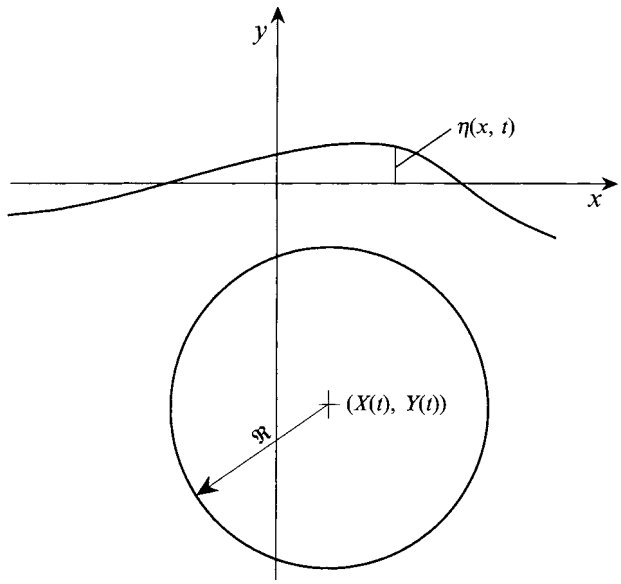

FIGURE 1. Definition sketch of the moving cylinder and free surface.

where $\boldsymbol{i}$ and $\boldsymbol{j}$ are unit vectors in the x- and y-directions, respectively. In (2.7) the position of the cylinder centre is written as

$$\boldsymbol{R}(t) = X(t)\,\boldsymbol{i} + Y(t)\boldsymbol{j}. \tag{2.9}$$

This position is prescribed by the forced motion of the cylinder. The exact boundary condition at the cylinder (2.7) will be expanded in time in the following section. Recently Wu (1993) has incorporated this exact condition into the wave radiation problem for an oscillating circular cylinder, but in contrast to the present work, the free-surface conditions were linearized. Our initial conditions are chosen as

$$\eta(x, 0) = 0, \tag{2.10}$$

$$\Phi(x, 0, 0) = 0. \tag{2.11}$$

These conditions imply that the free surface is initially undisturbed, and that the motion is started impulsively during an infinitesimal time interval. Since all velocities are finite during the impulsive start, (2.10) and (2.11) arise from integrating (2.5) and (2.6) over the infinitesimal time interval of the impulsive start.

We choose ρW^2 as a reference pressure. The pressure (p) is given by Bernoulli's equation, which has a form consistent with the dynamic boundary condition (2.6):

$$p + \frac{\partial \Phi}{\partial t} + \tfrac{1}{2}|\nabla \Phi|^2 + Fr^{-2} y = 0. \tag{2.12}$$

In accordance with our previous choices of dimensionless quantities, the units of dimensionless mass, force and momentum (per length along the cylinder) are given by (ρD^2), ($\rho D W^2$) and ($\rho D^2 W$), respectively. The physical meaning of the latter is the momentum of a unit-square cylinder of fluid moving with the unit velocity. This is not to be confused with the scale for the added momentum at the initial instant: the appropriate scale is the momentum of a fluid mass displaced by the cylinder, when it

moves with the initial velocity. The dimensionless value of this momentum scale is $(\pi\epsilon^2)$, being the same as the added momentum of a cylinder in infinite fluid.

3. The small-time expansion

Our full nonlinear initial/boundary value problem consists of (2.3)–(2.7), and (2.10)–(2.11). These equations are solved analytically by employing a small-time expansion (e.g. Peregrine 1972; Greenhow & Lin 1983). We then postulate

$$(\Phi, \eta, \boldsymbol{R}) = (0, 0, \boldsymbol{R}_0) + H(t)[(\Phi_0, 0, 0) + t(\Phi_1, \eta_1, \boldsymbol{R}_1) + t^2(\Phi_2, \eta_2, \boldsymbol{R}_2) + \ldots] \quad (-\infty < t < \infty). \tag{3.1}$$

We prefer to write this equation in a form common for all times, negative as well as positive. Therefore the Heaviside unit step function $H(t)$ has been introduced:

$$H(t) = 0, \quad t \leqslant 0 \quad \text{and} \quad H(t) = 1, \quad t > 0. \tag{3.2}$$

The asymptotic series (3.1) will diverge for times exceeding some value of order 1: our expansion aims to extrapolate the whole solution from the initial locations of the cylinder and free surface, but such a procedure cannot be valid when the cylinder is displaced further than its own initial submergence depth. In (3.1) Φ_n and η_n are unknown functions, whereas the instantaneous position vector of the cylinder centre is prescribed by its forced motion:

$$\boldsymbol{R}_n = \boldsymbol{i}X_n + \boldsymbol{j}Y_n \quad (n = 0, 1, 2, \ldots), \tag{3.3}$$

where we have already defined

$$(X_0, Y_0) = (0, -1). \tag{3.4}$$

From the series expansion of the velocity potential it follows immediately that the governing equations are

$$\nabla^2\Phi_n = 0, \quad y < 0, \quad x^2 + (y+1)^2 > \epsilon^2, \tag{3.5}$$

expressing the potential flow to each order in the initial fluid domain. The corresponding far-field conditions are

$$|\nabla\Phi_n| \to 0, \quad x^2 + y^2 \to \infty \quad (n = 0, 1, 2, \ldots). \tag{3.6}$$

The operator of total time differentiation at the moving free surface is

$$\left(\frac{\mathrm{d}}{\mathrm{d}t}\right)_{surface} = \frac{\partial}{\partial t} + \frac{\partial\eta}{\partial t}\frac{\partial}{\partial y}. \tag{3.7}$$

The free-surface conditions to each order are found from (2.5) and (2.6) by applying the operator (3.7) recursively and putting $t = 0$ in the resulting small-time expansions (see e.g. Tyvand 1991). The resulting dynamic conditions are given below:

$$\Phi_0 = 0, \quad y = 0, \tag{3.8}$$

$$\Phi_1 = -\tfrac{1}{2}\eta_1^2, \quad y = 0, \tag{3.9}$$

$$\Phi_2 = -\eta_1(2\eta_2 + \tfrac{1}{2}Fr^{-2}), \quad y = 0. \tag{3.10}$$

So far, we have stated the general dynamic conditions. But for the third-order potential we give only the version valid for constant acceleration from rest:

$$\Phi_3 = -\tfrac{1}{3}\eta_2(4\eta_2 + Fr^{-2}), \quad y = 0. \tag{3.11}$$

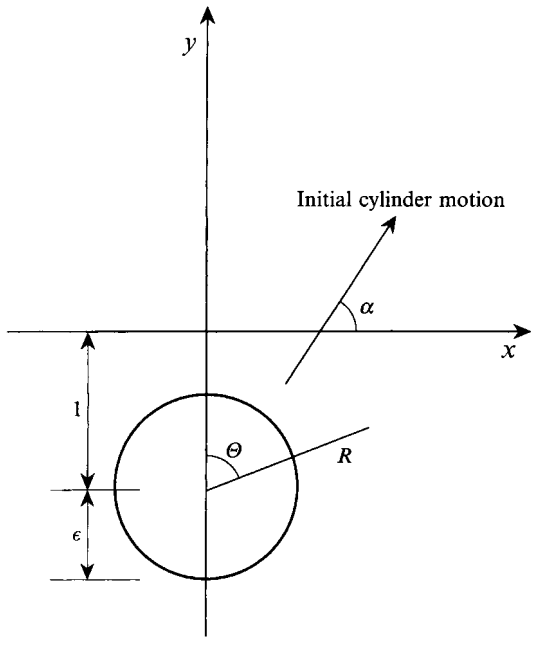

FIGURE 2. Initial position of the cylinder. Dimensionless lengths and polar coordinates (R, Θ).

The corresponding kinematic conditions are

$$\eta_1 = \partial\Phi_0/\partial y, \quad y = 0, \tag{3.12}$$

$$2\eta_2 = \partial\Phi_1/\partial y, \quad y = 0, \tag{3.13}$$

$$6\eta_3 = 2\partial\Phi_2/\partial y + \eta_1^2\eta_1'' + 2\eta_1(\eta_1')^2, \quad y = 0, \tag{3.14}$$

$$4\eta_4 = \partial\Phi_3/\partial y, \quad y = 0. \tag{3.15}$$

These kinematic conditions are also general, except for the last one, which is only valid for the case of constant acceleration. The general versions of conditions (3.11) and (3.15) are considerably more complicated, and contain many terms representing interactions between the first-, second- and third-order elevations.

In (3.14) the prime denotes $(\mathrm{d}/\mathrm{d}x)$. We carry our perturbation scheme this far because we want to include the leading-order gravitational effects in the case of constant acceleration from rest. All free-surface boundary conditions, i.e. (3.8)–(3.15), have been written concisely by introducing lower-order surface elevations wherever possible. We perform a simultaneous extrapolation of both the free surface and the cylinder location out from their initial positions. We introduce polar coordinates (R, Θ) with origin in the initial cylinder centre $(0, -1)$:

$$(x, y+1) = R(\sin\Theta, \cos\Theta). \tag{3.16}$$

Thus we let Θ measure the clockwise angle out from the vertical y-axis ($-\pi \leqslant \Theta < \pi$). See figure 2. This unconventional definition of polar coordinates has been chosen in order to correspond to the bipolar coordinates which will be introduced in the next section. In figure 2 we also introduce the angle α between the initial velocity vector and the x-axis.

Our task is now to expand the exact boundary condition (2.7) at the cylinder contour in powers of t. This is done by successively applying the operator of total time differentiation following the cylinder in its motion:

$$\left(\frac{\mathrm{d}}{\mathrm{d}t}\right)_{cylinder} = \frac{\partial}{\partial t} + \dot{\boldsymbol{R}}\cdot\boldsymbol{\nabla}. \tag{3.17}$$

After each application of this operator, we insert the series (3.1) for Φ, and then set $t = 0$. We introduce the radial unit vector, which is evaluated at the initial cylinder contour:

$$\boldsymbol{i}_R = \boldsymbol{i}\sin\Theta + \boldsymbol{j}\cos\Theta. \tag{3.18}$$

The zeroth-order condition may then be written

$$\partial\Phi_0/\partial R = \boldsymbol{R}_1\cdot\boldsymbol{i}_R, \quad R = \epsilon. \tag{3.19}$$

We also give the full first- and second-order conditions:

$$\partial\Phi_1/\partial R = 2\boldsymbol{R}_2\cdot\boldsymbol{i}_R - \boldsymbol{i}_R\cdot\boldsymbol{\nabla}(\boldsymbol{R}_1\cdot\boldsymbol{\nabla}\Phi_0), \quad R = \epsilon, \tag{3.20}$$

$$\frac{2\partial\Phi_2}{\partial R} = 3\boldsymbol{R}_3\cdot\boldsymbol{i}_R - 2\boldsymbol{i}_R\cdot\boldsymbol{\nabla}(\boldsymbol{R}_2\cdot\boldsymbol{\nabla}\Phi_0)$$

$$-2\boldsymbol{i}_R\cdot\boldsymbol{\nabla}(\boldsymbol{R}_1\cdot\boldsymbol{\nabla}\Phi_1) - \boldsymbol{i}_R\cdot\boldsymbol{\nabla}(\boldsymbol{R}_1\cdot\boldsymbol{\nabla}(\boldsymbol{R}_1\cdot\boldsymbol{\nabla}\Phi_0)), \quad R = \epsilon. \tag{3.21a}$$

One notes that the right-hand-side inhomogeneities of these boundary conditions do not contain any explicit Froude number dependence. This implies that the leading-order gravity-dependent potential will satisfy the condition of zero normal derivative at the cylinder contour. When the cylinder moves with a constant velocity we thus get

$$\partial\Phi_2^{(Fr)}/\partial R = 0, \quad R = \epsilon \tag{3.21b}$$

as a special case of the previous condition. Here we have introduced the superscript (Fr) to denote the gravity-dependent contribution. In our second special case of a constant acceleration (starting from rest; see § 10), the full third-order condition at the cylinder contour becomes rather simple:

$$\partial\Phi_3/\partial R = -\tfrac{2}{3}\boldsymbol{i}_R\cdot\boldsymbol{\nabla}(\boldsymbol{R}_2\cdot\boldsymbol{\nabla}\Phi_1), \quad R = \epsilon. \tag{3.22}$$

Within each order of the series expansion, the principle of superposition is valid. Therefore we may split the potential into two contributions at each order, i.e.

$$\Phi_n = \phi_n + \psi_n \quad (n = 0, 1, 2, \ldots). \tag{3.23}$$

The first term (ϕ_n) is generated by the inhomogeneous condition at the free surface with zero normal derivative at the cylinder contour. The second term (ψ_n) is generated by the inhomogeneous boundary condition at the cylinder contour, with a homogeneous condition at the free surface. The small-cylinder theory of our accompanying paper (Tyvand & Miloh 1995, equation 4.2) represents ψ_n as a moving-dipole potential: it is prescribed explicitly, and has been used to check the validity of our present first-order condition (3.20) at the cylinder contour.

Expressed in terms of the polar coordinates, we represent the dimensionless integral for the force exerted on the cylinder by the surrounding fluid as

$$\boldsymbol{F} = -\epsilon\int_{-\pi}^{\pi} p(\epsilon, \Theta)\,\boldsymbol{i}_R\,\mathrm{d}\Theta. \tag{3.24}$$

From Bernoulli's equation (2.12), the above pressure integral produces a small-time expansion for the hydrodynamic force with an extra singular term:

$$\boldsymbol{F} = \boldsymbol{F}_{-1}\,\delta(t) + (\boldsymbol{F}_0 + \boldsymbol{F}_1\,t + \boldsymbol{F}_2\,t^2 + \ldots)\,H(t). \tag{3.25}$$

Here $\delta(t)$ is Dirac's delta function, which is the derivative of the Heaviside unit step function $H(t)$. By integrating the force in time, we find the force-impulse exerted on the cylinder during its impulsive start:

$$\Delta\boldsymbol{P} = \int_{-\infty}^{0^+} \boldsymbol{F}\,\mathrm{d}t = \boldsymbol{F}_{-1}. \tag{3.26}$$

Its magnitude is equal to the added momentum accumulated around the cylinder during the infinitesimal time interval of an impulsive start. The constant hydrostatic force,

$$\boldsymbol{F}_{static} = \pi(\epsilon/Fr)^2\boldsymbol{j}, \tag{3.27}$$

is omitted in our force calculations, since, unlike the other contributions, it is not turned on at time zero.

The principle of mass conservation implies that the integral of the surface elevation must be zero to each order:

$$\int_{-\infty}^{\infty} \eta_n\,\mathrm{d}x = 0 \quad (n = 1, 2, \ldots). \tag{3.28}$$

4. Bipolar coordinates

We will solve the exact boundary value problem to each order by means of bipolar coordinates. The bipolar coordinate system is described in the books by Morse & Feshbach (1953, p. 1210) and Moon & Spencer (1988, p. 89). Figure 3 gives a sketch of our domain of computation as represented by the bipolar coordinates ζ and θ. All quantities are made dimensionless.

An attractive feature of the bipolar coordinate system is that Laplace's equation separates into

$$\left(\frac{\partial^2}{\partial\zeta^2} + \frac{\partial^2}{\partial\theta^2}\right)\Phi = 0. \tag{4.1}$$

The transformation between the Cartesian and the bipolar coordinate system (ζ, θ) is given by

$$x = \frac{a\sin\theta}{\cosh\zeta + \cos\theta}, \tag{4.2}$$

$$y = -\frac{a\sinh\zeta}{\cosh\zeta + \cos\theta}. \tag{4.3}$$

The scale factors of the transformation from Cartesian to bipolar coordinates are (being the square root of the Jacobian)

$$h_\zeta = h_\theta = \frac{a}{\cosh\zeta + \cos\theta}. \tag{4.4}$$

Our domain of computation is the undisturbed fluid domain defined by

$$-\pi < \theta < \pi \quad \text{and} \quad 0 < \zeta < \zeta_0. \tag{4.5}$$

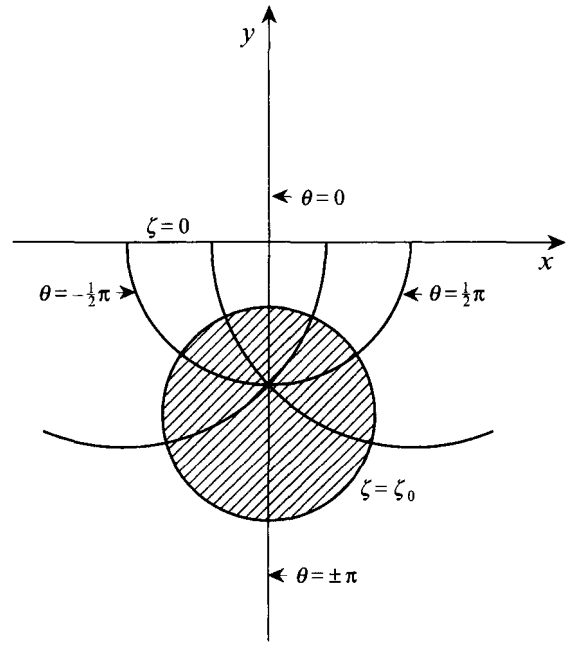

FIGURE 3. Definition sketch for bipolar coordinates (ζ, θ).

Here a is a dimensionless length, representing the centres $(x, y) = (0, \pm a)$ of the bipolar coordinate system. It is related to the radius through

$$a = (1-\epsilon^2)^{1/2}. \tag{4.6}$$

One can also express the cylinder radius, using these new parameters, as

$$\epsilon = \frac{a}{\sinh \zeta_0} = (\cosh \zeta_0)^{-1} = \operatorname{sech} \zeta_0. \tag{4.7}$$

It is natural to first specify a value for ϵ. The corresponding values for ζ_0 and a are given by

$$\zeta_0 = \operatorname{arcsech} \epsilon, \quad a = \tanh \zeta_0. \tag{4.8}$$

In the boundary-value problems we will perform transformations from Θ to θ at the cylinder contour. So we derive two equations for the one-to-one transformation between Θ and θ:

$$\sin \Theta = \frac{\sinh \zeta_0 \sin \theta}{\cosh \zeta_0 + \cos \theta}, \quad \cos \Theta = \frac{1 + \cosh \zeta_0 \cos \theta}{\cosh \zeta_0 + \cos \theta}. \tag{4.9a, b}$$

By differentiating the first of these relationships, we find a relationship between the differentials at the cylinder contour:

$$\frac{\mathrm{d}\Theta}{\mathrm{d}\theta} = \frac{\sinh \zeta_0}{\cosh \zeta_0 + \cos \theta} = \frac{\sin \Theta}{\sin \theta}. \tag{4.10}$$

This also means that $\tan(\frac{1}{2}\Theta)$ is proportional to $\tan(\frac{1}{2}\theta)$. Equations (4.9) and (4.10) are valid only along the cylinder contour.

5. The zeroth-order potential and first-order elevation

The inhomogeneous boundary condition (3.19) for the zeroth-order potential is expressed in bipolar coordinates as

$$\frac{\partial \Phi_0}{\partial \zeta}(\zeta_0, \theta) = -h_\zeta \frac{\partial \Phi_0}{\partial R}(\epsilon, \Theta) = -\frac{a \sin(\Theta + \alpha)}{\cosh \zeta_0 + \cos \theta}, \tag{5.1}$$

where α is defined as the angle between the initial velocity vector and the x-axis:

$$X_1 = \cos \alpha, \quad Y_1 = \sin \alpha. \tag{5.2}$$

In order to find the zeroth-order flow, we need to eliminate Θ from the boundary condition.

Next, we insert (4.9) into the boundary condition (5.1):

$$\frac{\partial \Phi_0}{\partial \zeta}(\zeta_0, \theta) = -a \frac{\sinh \zeta_0 \sin \theta \cos \alpha + (1 + \cosh \zeta_0 \cos \theta) \sin \alpha}{(\cosh \zeta_0 + \cos \theta)^2}. \tag{5.3}$$

In Appendix A the Fourier expansion of this boundary condition is derived. The solution satisfying the homogeneous free-surface condition (3.7) and the far-field condition (3.5) is then given by

$$\Phi_0 = 2 \tanh \zeta_0 \sum_{n=1}^{\infty} \frac{(-1)^n \mathrm{e}^{-n\zeta_0} \sin(n\theta + \alpha) \sinh n\zeta}{\cosh n\zeta_0}. \tag{5.4}$$

The first-order elevation (3.12) is expressed in bipolar coordinates as

$$\begin{aligned} \eta_1 &= -\frac{1}{h_\zeta} \frac{\partial \Phi_0}{\partial \zeta}(0, \theta) \\ &= 4 \cos^2(\tfrac{1}{2}\theta) \sum_{n=1}^{\infty} (-1)^{n+1} n \mathrm{e}^{-n\zeta_0} \operatorname{sech} n\zeta_0 \sin(n\theta + \alpha). \end{aligned} \tag{5.5}$$

A comparison of the exact first-order elevation (5.5) with the small-cylinder limit is given by Tyvand & Miloh (1995). In the present paper we display the first-order elevation as a function of the horizontal coordinate x. Using the definitions of the bipolar coordinate system we obtain the following transformation to be inserted into (5.5):

$$\theta = 2 \arctan\left(\frac{x}{\tanh \zeta_0}\right), \quad y = 0. \tag{5.6}$$

In figure 4 we show the first-order surface elevation as a function of x for three dimensionless radii: $\epsilon = 0.5$, 0.8 and 0.98. Figure 4(*a*) represents vertical motion ($\alpha = \frac{1}{2}\pi$), and figure 4(*b*) represents horizontal motion ($\alpha = 0$). This figure is based on the exact analytical solution (5.5), truncated to 40 terms in the Fourier series by MATHEMATICA®. We do not present here a figure for oblique motion, since its elevation is obtained by superposing the horizontal and vertical motion.

For our higher-order analysis it proves useful to rewrite the first-order elevation in the form

$$\eta_1 = \sum_{n=1}^{\infty} (-1)^{n+1} n \mathrm{e}^{-n\zeta_0} \frac{\sin[(n-1)\theta + \alpha] + 2 \sin(n\theta + \alpha) + \sin[(n+1)\theta + \alpha]}{\cosh n\zeta_0}. \tag{5.7}$$

For vertical initial motion ($\alpha = \frac{1}{2}\pi$) it is clear that the free-surface velocity in a neighbourhood around $x = 0$ ($\theta = 0$) must be slightly below 1 when ϵ is close to 1: then

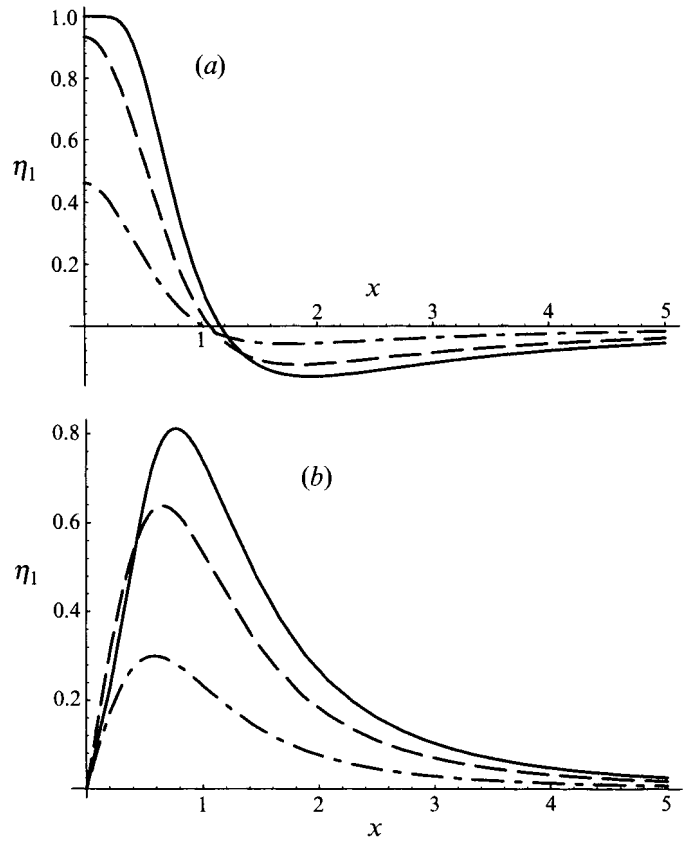

FIGURE 4. First-order surface elevation for three choices of dimensionless radius: $\epsilon = 0.5$ (dash-dot curves, smallest amplitude), $\epsilon = 0.8$ (dashed curves, medium amplitude), $\epsilon = 0.98$ (solid curves, largest amplitude). (*a*) Vertical motion ($\alpha = \frac{1}{2}\pi$). (*b*) Horizontal motion ($\alpha = 0$).

there is a shallow fluid layer that moves upwards with the cylinder. The early horizontal flow in this shallow layer must be comparatively weak. Our results confirm that the surface shape is relatively flat around $x = 0$ when ϵ is close to 1. In the small-cylinder limit (Tyvand & Miloh 1995) the first-order elevation changes sign at $|x| = 1$. The point of zero elevation shifts slowly towards larger $|x|$ when ϵ increases.

It is not so obvious how the free surface will behave when the initial motion is horizontal ($\alpha = 0$), apart from the fact that the first-order elevation must be antisymmetric with respect to $x = 0$. Our results show that the maximum surface elevation will be of order 1 when ϵ approaches 1, which is physically plausible. The position of this maximum shifts slowly to larger x with increasing ϵ.

For vertical cylinder motion the largest slope of the free surface occurs for a value of x about 0.7, in the limit $\epsilon \to 1$. The larger the cylinder, the steeper the maximum slope. For a cylinder in horizontal motion the maximum slope of the first-order elevation will always occur at $x = 0$. However, this maximum slope is not steepest in the limit $\epsilon \to 1$, as with slightly smaller cylinders: here, the steepest slope occurs when ϵ is roughly equal to 0.8. This indicates that there exists an optimal cylinder size for generating breaking waves. With the impulsive start of a cylinder in steady horizontal motion, there should be a minimum Froude number that will lead to surface breaking. Our results so far indicate that this minimum Froude number will correspond to a cylinder radius ϵ which is significantly smaller than one.

6. The added momentum during the impulsive start

From §§2 and 3 it follows that the dimensionless added momentum (or impulse) acquired by the cylinder during the impulsive start is given (in polar coordinates) by

$$\boldsymbol{F}_{-1} = \epsilon \int_{-\pi}^{\pi} \Phi_0(\epsilon, \Theta)\, \boldsymbol{i}_R \, \mathrm{d}\Theta. \tag{6.1}$$

Rewriting this integral in bipolar coordinates with Cartesian unit vectors yields

$$\begin{aligned} \boldsymbol{F}_{-1} &= \epsilon \int_{-\pi}^{\pi} \Phi_0(\zeta_0, \theta) \frac{\mathrm{d}}{\mathrm{d}\theta}\left(\frac{-\boldsymbol{i}(1+\cosh\zeta_0\cos\theta)+\boldsymbol{j}\sinh\zeta_0\sin\theta}{\cosh\zeta_0+\cos\theta}\right)\mathrm{d}\theta \\ &= 2\tanh^2\zeta_0 \sum_{n=1}^{\infty} (-1)^n \mathrm{e}^{-n\zeta_0}\tanh n\zeta_0 \\ &\quad \times \int_{-\pi}^{\pi} \sin(n\theta+\alpha)\frac{(\sinh\zeta_0\sin\theta)\,\boldsymbol{i}+(1+\cosh\zeta_0\cos\theta)\boldsymbol{j}}{(\cosh\zeta_0+\cos\theta)^2}\mathrm{d}\theta. \end{aligned} \tag{6.2}$$

In order to be able to evaluate this last integral, we first apply the Fourier expansions (A 2) and (A 3), where the summation index is now m. However, the only contributions to this force arise from $m = n$. Thus the final result is

$$\boldsymbol{F}_{-1} = -4\pi \boldsymbol{R}_1 \tanh^2\zeta_0 \sum_{n=1}^{\infty} n\mathrm{e}^{-2n\zeta_0}\tanh n\zeta_0. \tag{6.3}$$

By virtue of (5.2) we have introduced here the initial velocity

$$\boldsymbol{R}_1 = \boldsymbol{i}\cos\alpha + \boldsymbol{j}\sin\alpha. \tag{6.4}$$

The force impulse (6.3) represents the added momentum of the fluid surrounding the cylinder. It can also be expressed as the initial velocity times the (initial) added mass. Since this force always points in the direction opposite to the initial velocity, the added masses for heave and sway are identical, with the zero-potential condition applied at the free surface. This conclusion is in agreement with the linear analysis of Ogilvie (1963), who proved that added masses for heave and sway are always identical for submerged circular cylinders oscillating at any frequency. Our zero-potential condition at zeroth order coincides with the infinite-frequency limit of linear theory.

Greenhow & Li (1987) derived a general formula for the added mass of a circular cylinder near a free surface in the zero-potential limit. In their figure 2 they depicted the ratio (added mass)/(displaced fluid mass) as a function of the inverse radius ϵ^{-1} (using our notation). This is reproduced again in our figure 5, showing the added mass relative to the displaced mass,

$$|\boldsymbol{F}_{-1}|/(\pi\epsilon^2) = 4\sinh^2\zeta_0 \sum_{n=1}^{\infty} n\mathrm{e}^{-2n\zeta_0}\tanh n\zeta_0, \tag{6.5}$$

as a function of $\epsilon^{-1} = \cosh\zeta_0$. The summation is truncated after 50 terms. Our curve is in good agreement with that of Greenhow & Li (1987, figure 2). Similar results were found by Venkatesan (1985): his figure 1 represents the added mass of each of two equal cylinders performing transverse relative motion. (This is physically equivalent to the added mass of one submerged cylinder subject to the zero-potential free-surface condition.)

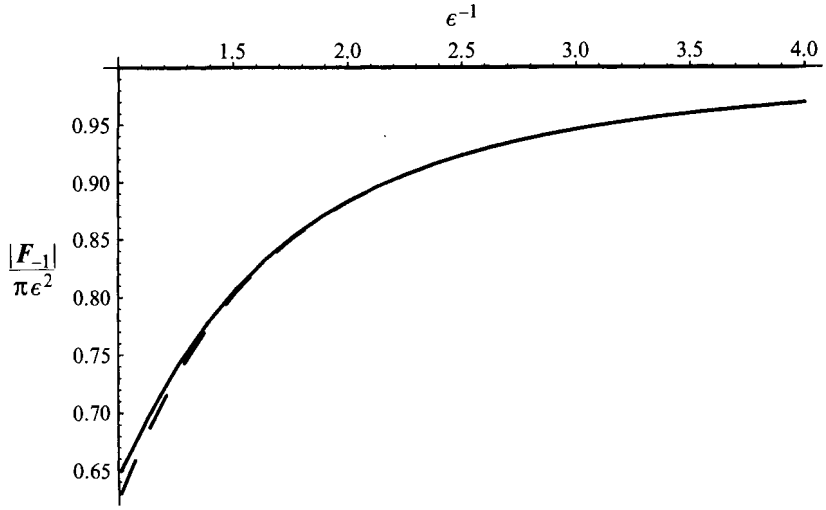

FIGURE 5. Added momentum during the impulsive start, expressed by the ratio of added mass to displaced fluid mass ($\pi\epsilon^2$), and given as a function of the inverse radius. Solid curve: exact Fourier series solution (6.5), truncated to 50 terms. Dashed curve: three-term asymptotic expansion (6.6), valid in the small-cylinder limit.

Tyvand & Miloh (1995) derives the asymptotic expansion valid for small ϵ:

$$|F_{-1}|/(\pi\epsilon^2) = 1 - \tfrac{1}{2}\epsilon^2 + \tfrac{1}{8}\epsilon^4. \tag{6.6}$$

The graphical representation of (6.6) follows very closely the exact curve (6.5) for all $\epsilon^{-1} > 1.5$, and is included in our figure 5 (dashed curve).

7. The first-order potential and second-order elevation

The potential ϕ_1 is the leading-order contribution due to the nonlinearity at the free surface. It is calculated in Appendix B, from which we find that its contribution to the second-order surface elevation is

$$\begin{aligned}\frac{1}{2}\frac{\partial\phi_1}{\partial y}(y=0) &= -\frac{1}{2h_\zeta}\frac{\partial\phi_1}{\partial\zeta}(0,\theta)\\ &= \frac{\cos^2(\frac{1}{2}\theta)}{16\tanh\zeta_0}\sum_{n=1}^{\infty}\sum_{m=1}^{\infty}(-1)^{n+m}\,nm\,\mathrm{e}^{-(n+m)\zeta_0}\operatorname{sech} n\zeta_0\operatorname{sech} m\zeta_0\\ &\quad\times\sum_{k=-2}^{2}(24-9k^2+k^4)\sum_{q=-1}^{1}q(n+qm+k)\cos((n+qm+k)\theta+(q+1)\alpha)\\ &\quad\times\tanh(n+qm+k)\zeta_0.\end{aligned} \tag{7.1}$$

Figure 6 shows this second-order elevation due to the free-surface nonlinearity, given by (7.1), for the same three values of the radius as in figure 4. Figure 6(*a*) shows the elevation for vertical motion, and figure 6(*b*) shows the elevation for horizontal motion. Both of these curves are symmetric with respect to $x = 0$. However, no values of α between 0 and $\frac{1}{2}\pi$ gives any symmetry with respect to $x = 0$. Owing to nonlinear interaction (in this second-order elevation) between horizontal and vertical cylinder motion, these asymmetric surface shapes cannot be deduced from those of purely horizontal or vertical motion.

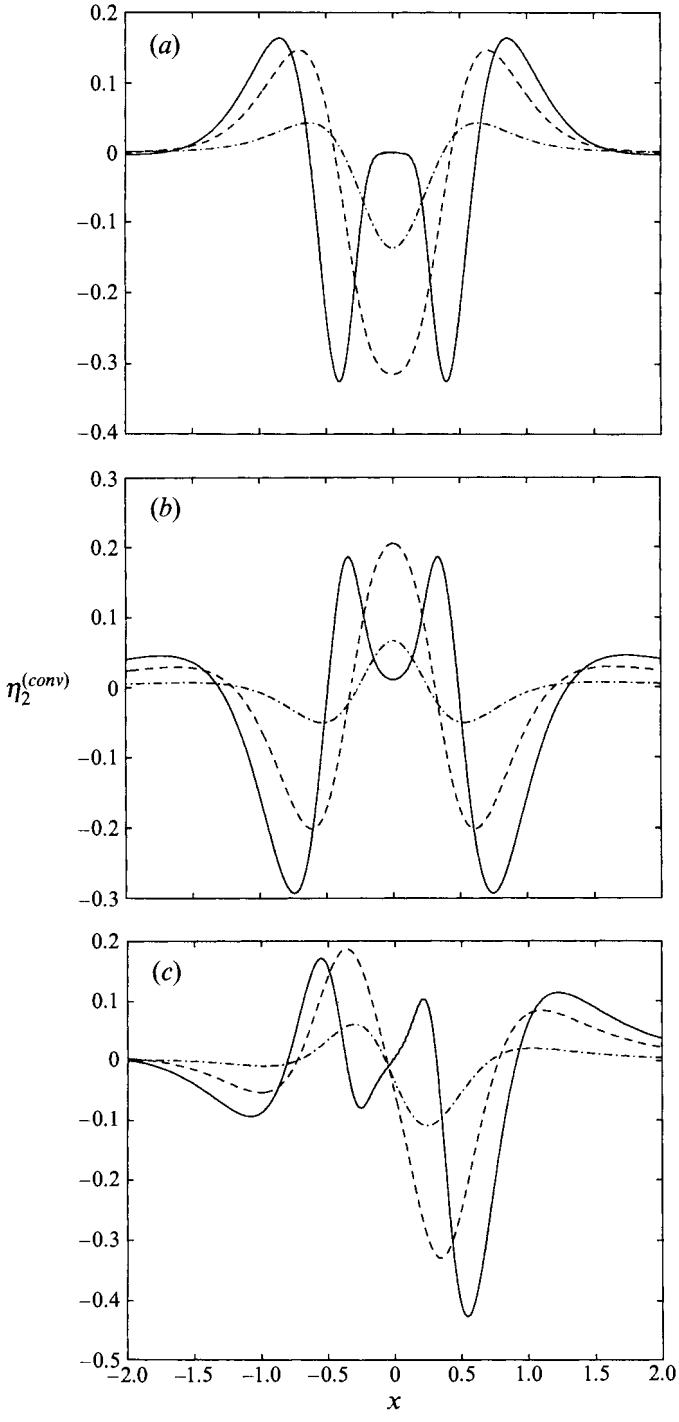

FIGURE 6. Second-order surface elevation due to convective acceleration at the free surface; $\eta_2^{(conv)}(x) = \frac{1}{2}(\partial\phi_1/\partial y)_{y=0}$. The exact Fourier series solution (7.1) has been truncated after 20 terms in both n and m. Dash-dot curves: $\epsilon = 0.5$. Dashed curves: $\epsilon = 0.8$. Solid curves: $\epsilon = 0.98$. (*a*) Vertical motion ($\alpha = \frac{1}{2}\pi$). (*b*) Horizontal motion ($\alpha = 0$). (*c*) Oblique motion ($\alpha = \frac{1}{4}\pi$).

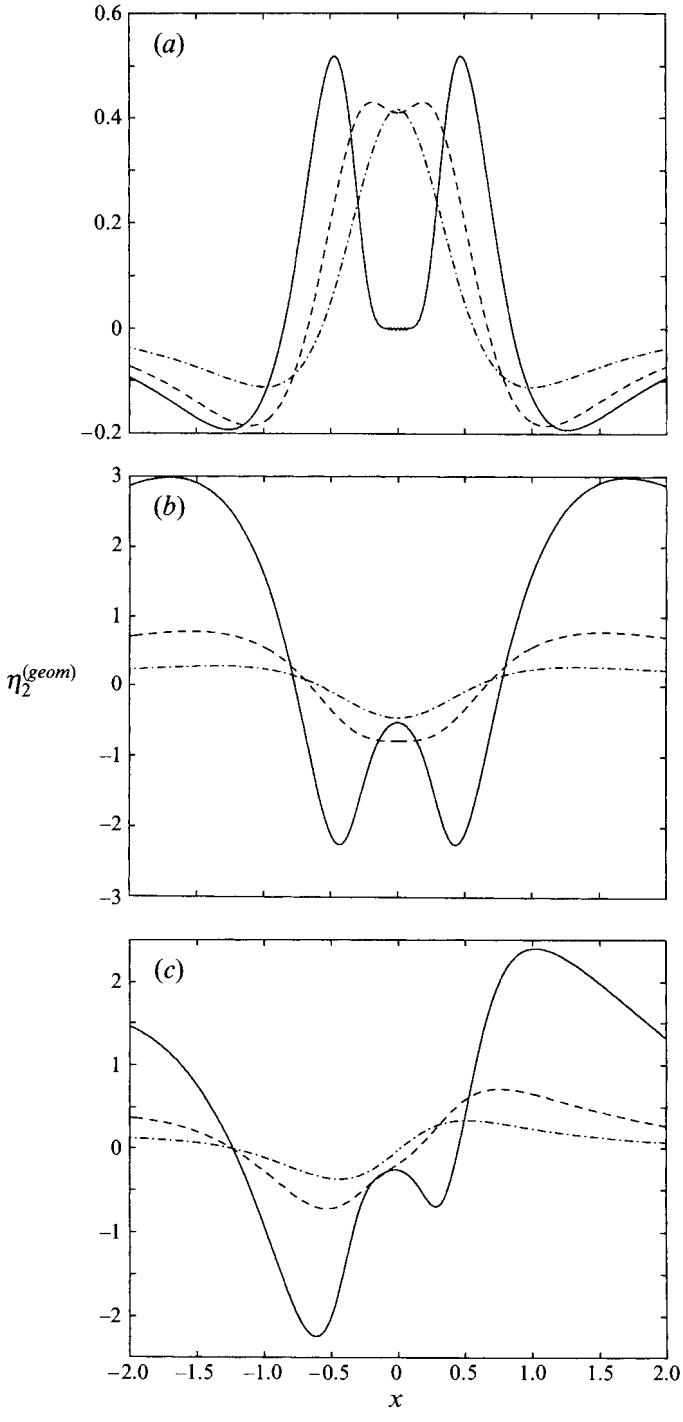

FIGURE 7. Second-order surface elevation due to geometric nonlinearity; $\eta_2^{(geom)}(x) = \frac{1}{2}(\partial\psi_1/\partial y)_{y=0}$. The exact Fourier series solution (7.3) has been truncated after 20 terms in both n and m. Dash-dot curves: $\epsilon = 0.5$. Dashed curves: $\epsilon = 0.8$. Solid curves: $\epsilon = 0.98$. (*a*) Vertical motion ($\alpha = \frac{1}{2}\pi$). (*b*) Horizontal motion ($\alpha = 0$). (*c*) Oblique motion ($\alpha = \frac{1}{4}\pi$).

Figure 6 (*c*) shows the second-order elevation due to the free-surface nonlinearity for the case $\alpha = \frac{1}{4}\pi$ (oblique motion). When the motion is oblique, there is never exact antisymmetry about $x = 0$, even in the small-cylinder limit. In the present case ($\alpha = \frac{1}{4}\pi$) the deepest surface trough is always deeper than the highest surface crest.

The potential ψ_1 is the leading-order contribution due to geometric nonlinearity at the cylinder contour. It is calculated in Appendix B. Its contribution to the second-order surface elevation may be expressed concisely by a mixture of Cartesian and biharmonic coordinates:

$$\frac{1}{2}\frac{\partial \psi_1}{\partial y}(y=0) = -\frac{1}{2h_\zeta}\frac{\partial \tilde{\psi}_1}{\partial \zeta}(0,\theta) - \tfrac{1}{2}\cos\alpha \frac{\mathrm{d}\eta_1}{\mathrm{d}\theta}\frac{\mathrm{d}\theta}{\mathrm{d}x}(y=0). \tag{7.2}$$

The function $\tilde{\psi}_1$ is defined in (B 9). We insert (5.4)–(5.7) and find a Fourier series solution for the second-order elevation due to geometric nonlinearity:

$$\begin{aligned}\frac{1}{2}\frac{\partial \psi_1}{\partial y}(y=0) = &-\sin\alpha \frac{\cos^2(\frac{1}{2}\theta)}{\tanh\zeta_0}\sum_{n=1}^{\infty}(-1)^n n\,\mathrm{e}^{-n\zeta_0}\operatorname{sech} n\zeta_0 \\ &\times((n-1)\sin((n-1)\theta+\alpha)\tanh(n-1)\zeta_0 + 2n\sin(n\theta+\alpha)\tanh n\zeta_0 \\ &+(n+1)\sin((n+1)\theta+\alpha)\tanh(n+1)\zeta_0) \\ &-\frac{2\cos\alpha}{\tanh\zeta_0 + x^2}\sum_{n=1}^{\infty}(-1)^n n\,\mathrm{e}^{-n\zeta_0}\operatorname{sech} n\zeta_0 \\ &\times[\sin\theta\sin(n\theta+\alpha) - 2n\cos^2(\tfrac{1}{2}\theta)\cos(n\theta+\alpha)].\end{aligned} \tag{7.3}$$

In the last fraction we may replace x^2 by $[\tanh^2\zeta_0 \tan^2(\frac{1}{2}\theta)]$, to obtain an expression with bipolar coordinates alone.

We first note that the second-order elevation for a given cylinder is unchanged when its direction of motion is reversed (i.e. the angle α in (7.1) and (7.3) is replaced by $-\alpha$). This implies that an asymmetry between upward and downward motion will evolve after a finite time: the surface mound above a given cylinder in upward motion grows larger than the depth of the surface trough above the same cylinder in downward motion. This asymmetry is primarily due to geometric nonlinearity, because the cylinder becomes more efficient in generating surface motion the closer it gets to the surface.

Figure 7 (*a–c*) shows the second-order surface elevation due to geometric nonlinearity (7.3), for the same values of ϵ and α as in figure 6. Their amplitudes are generally much larger than those due to the hydrodynamic nonlinearity at the free surface ((7.1) and figure 6), and they tend much more slowly to zero in the far field.

Figure 8 (*a–c*) shows the total second-order surface elevation, as the sum of the curves in figures 6 and 7. We see that most of the curves in figure 8 are fairly close to the corresponding curves in figure 7. However, for vertical motion ($\alpha = \frac{1}{2}\pi$) there are interesting peculiarities: at $\epsilon = 0.8$ there is a marked surface dip at $x = 0$ for the total elevation; at $\epsilon = 0.98$ there is a region ($-0.25 < x < 0.25$) where the total surface elevation is almost zero, but in the subintervals $0.15 < |x| < 0.25$ the contributions (7.1) and (7.3) tend to cancel each other instead of being zero separately. The region of zero second-order elevation represents a thin layer above the cylinder that passively follows its upward motion with unit velocity, see figure 4 (*a*).

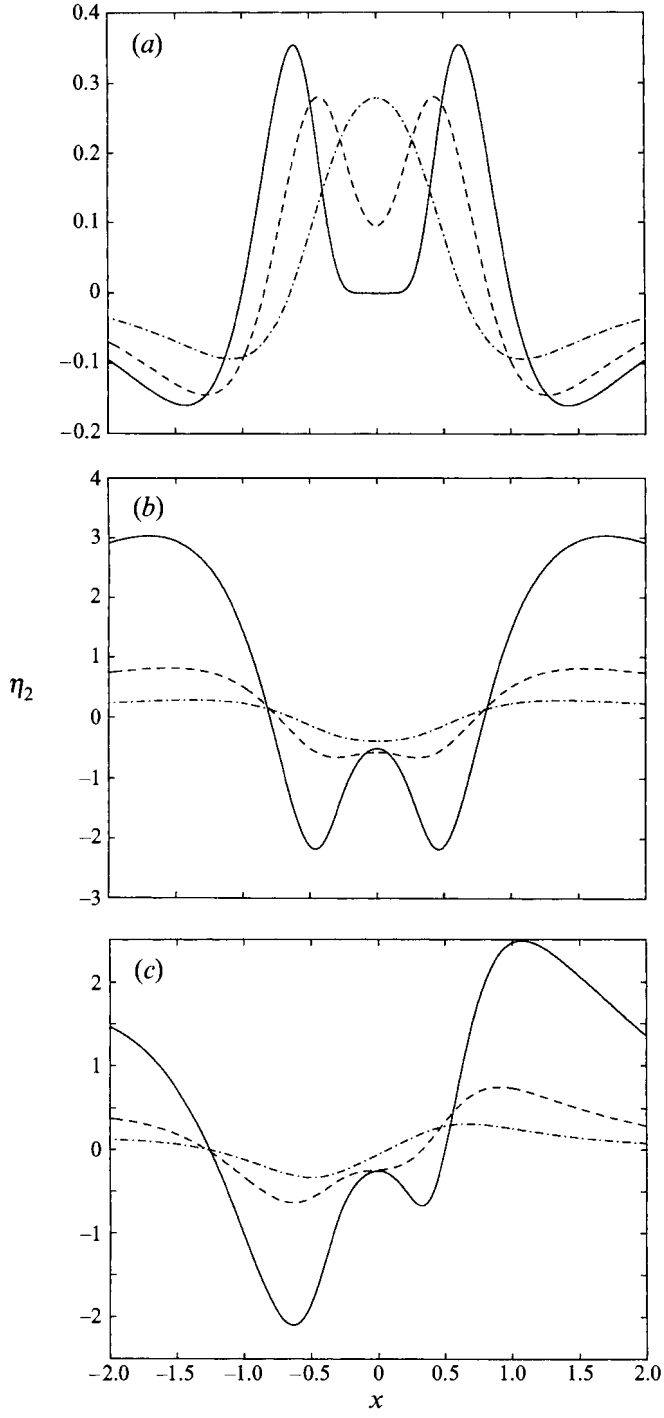

FIGURE 8. The total second-order surface elevation η_2 as a function of x. It is the sum of (7.1) and (7.3), as displayed in figures 6 and 7. Dash-dot curves: $\epsilon = 0.5$. Dashed curves: $\epsilon = 0.8$. Solid curves: $\epsilon = 0.98$. (*a*) Vertical motion ($\alpha = \frac{1}{2}\pi$). (*b*) Horizontal motion ($\alpha = 0$). (*c*) Oblique motion ($\alpha = \frac{1}{4}\pi$).

8. The zeroth-order hydrodynamic force

For a discussion of force calculations within the realm of small-time expansions, we refer to Miloh (1991*a*, *b*). We will now calculate the zeroth-order force, which is a time-independent force on the cylinder. This is the dominating force on the cylinder just after it has been forced impulsively into motion. The total zeroth-order force for constant speed ($X_2 = Y_2 = 0$) can be written (see §3)

$$\boldsymbol{F}_0 = \boldsymbol{F}_0^{(dyn)} + \boldsymbol{F}_0^{(free)} + \boldsymbol{F}_0^{(geom)}. \tag{8.1}$$

These three terms are defined in polar coordinates as

$$\boldsymbol{F}_0^{(dyn)} = \frac{1}{2\epsilon}\int_{-\pi}^{\pi}\left[\frac{\partial \Phi_0}{\partial \Theta}(\epsilon, \Theta)\right]^2 \boldsymbol{i}_R \,\mathrm{d}\Theta, \tag{8.2a}$$

$$\boldsymbol{F}_0^{(free)} = \epsilon\int_{-\pi}^{\pi} \phi_1(\epsilon, \Theta)\, \boldsymbol{i}_R \,\mathrm{d}\Theta, \tag{8.2b}$$

$$\boldsymbol{F}_0^{(geom)} = \epsilon\int_{-\pi}^{\pi} \psi_1(\epsilon, \Theta)\, \boldsymbol{i}_R \,\mathrm{d}\Theta, \tag{8.2c}$$

The zeroth-order force is the sum of three different effects: (i) the dynamic-pressure effect (superscript *dyn*) due to the zeroth-order tangential flow along the cylinder contour; (ii) the first-order flow due to the leading-order nonlinear effects of the convective acceleration at the free surface (superscript *free*); (iii) the geometric nonlinearity in the first-order flow (superscript *geom*), accounting for the fact that the cylinder centre is being displaced out from its initial position at any finite time since the start. In Appendix B we have separated out effects (ii) and (iii) by means of the two functions ϕ_1 and ψ_1.

In figures 9–11 we display the different force components defined by (8.2), for the cases $\alpha = 0$, $\frac{1}{4}\pi$ and $\frac{1}{2}\pi$.

Tyvand & Miloh (1995) derive the following expressions which may only be valid asymptotically in the small-cylinder limit:

$$\boldsymbol{F}_0^{(free)}/(\pi\epsilon^2) \sim (\tfrac{1}{4}\epsilon^4)[-\boldsymbol{i}\sin 2\alpha + \boldsymbol{j}(\cos 2\alpha - 2)], \tag{8.3}$$

$$\boldsymbol{F}_0^{(geom)}/(\pi\epsilon^2) \sim \epsilon^2 \boldsymbol{R}_1 \sin\alpha = \tfrac{1}{2}\epsilon^2[\boldsymbol{i}\sin 2\alpha + \boldsymbol{j}(1-\cos 2\alpha)]. \tag{8.4}$$

In our asymptotic small-cylinder theory (Tyvand & Miloh 1995) the force component due to the dynamic-pressure effect vanishes, because the flow surrounding the cylinder is considered as locally uniform. But now its exact formula is found in a way similar to that described in §6. This dynamic-pressure force points in the vertical direction:

$$\boldsymbol{F}_0^{(dyn)} = \boldsymbol{j}\pi \tanh\zeta_0 \sum_{n=1}^{\infty} n\,\mathrm{e}^{-2n\zeta_0}\tanh n\zeta_0[2n\tanh n\zeta_0 - ((n-1)\,\mathrm{e}^{\zeta_0}\tanh(n-1)\,\zeta_0 + (n+1)\,\mathrm{e}^{-\zeta_0}\tanh(n+1)\,\zeta_0)\cosh\zeta_0]. \tag{8.5}$$

This exact dynamic-pressure force divided by the dimensionless displaced fluid mass ($\pi\epsilon^2$) is displayed in figure 9, where the Fourier series (8.5) has been truncated to 100 terms and summed by MATHEMATICA. Its magnitude grows monotonically with the cylinder radius, and tends to a value about 0.08 as $\epsilon \to 1$. The dynamic-pressure force points downwards. This is again physically plausible: the initial streamlines will be closer together below the cylinder than above it, since the flow generated by the cylinder is vertical at the free surface. We note that the zeroth-order dynamic-pressure force is independent of the direction of the initial motion. For small ϵ we find

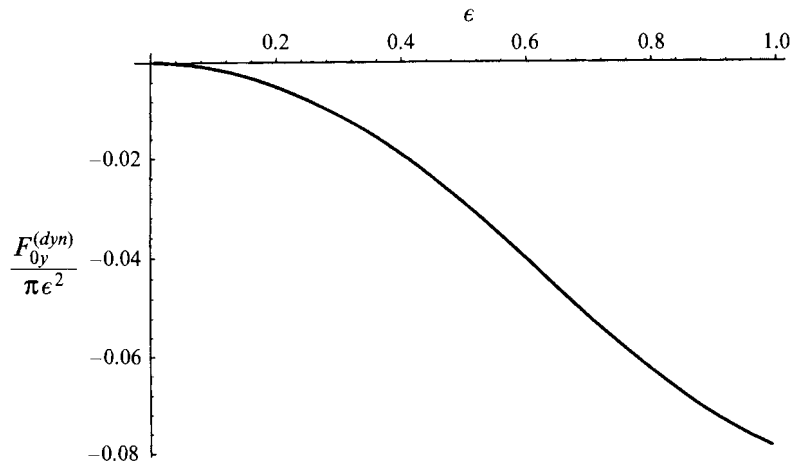

FIGURE 9. Dynamic-pressure force $F_{0y}^{(dyn)}$ divided by the displaced fluid mass ($\pi\epsilon^2$) and given as a function of the radius ϵ. The exact Fourier series (8.5) is truncated to 100 terms.

numerically that the dynamic-pressure force (8.5) is of order ϵ^4. Since this is the leading order of magnitude for the largest contributions to the zeroth-order force, we see that our small-cylinder asymptotic expansion (Tyvand & Miloh 1995) can never be fully consistent with respect to the total zeroth-order force.

More generally, a theory for the steady force like that of Greenhow (1988, equation 1), based on the time derivative of the momentum (with a zero-potential free-surface condition) must always be conceptually incorrect. But its errors are small for purely vertical motion of a small cylinder, when the only mistake arises from the small dynamic-pressure force (8.5). The errors of such a theory will be much more serious for larger cylinders, especially if the motion has a horizontal component.

The force contribution due to the leading nonlinear free-surface effect is found to be

$$\begin{aligned} \boldsymbol{F}_0^{(free)} = {} & \tfrac{1}{8}\pi \tanh\zeta_0 \sum_{n=1}^{\infty}\sum_{m=1}^{\infty} \frac{(-1)^{n+m}\, nm\, \mathrm{e}^{-(n+m)\zeta_0}}{\cosh n\zeta_0 \cosh m\zeta_0} \\ & \times \sum_{k=-2}^{2} (24-9k^2+k^4) \sum_{q=-1}^{1} \frac{(-1)^{n+qm+k}\, q(n+qm+k)}{\cosh(n+qm+k)\zeta_0} \\ & \times [\mathrm{e}^{(n+qm+k)\zeta_0} H(-n-qm-k)(\boldsymbol{i}\sin(q+1)\alpha + \boldsymbol{j}\cos(q+1)\alpha) \\ & + \mathrm{e}^{-(n+qm+k)\zeta_0} H(n+qm+k)(\boldsymbol{i}\sin(q+1)\alpha - \boldsymbol{j}\cos(q+1)\alpha)]. \end{aligned} \tag{8.6}$$

The precise definition (3.2) is crucial for the correct evaluation of (8.6). In figure 10 we show these force components $F_{0x}^{(free)}$ (solid curves) and $F_{0y}^{(free)}$ (dashed curves) as functions of the cylinder radius ϵ for vertical, horizontal and oblique motion ($\alpha = \frac{1}{2}\pi$, 0, $\frac{1}{4}\pi$). In the diagrams the force components have been divided by ($\frac{1}{4}\pi\epsilon^6$), in order to allow a direct comparison with the asymptotic formula (8.3) valid in the small-cylinder limit. In all cases we find good agreement with the small-cylinder limit when $\epsilon < 0.1$. The horizontal force component exists only when the motion is oblique, and its magnitude is smaller than the corresponding vertical force.

The zeroth-order force due to the geometric nonlinearity is split into two contributions:

$$\boldsymbol{F}_0^{(geom)} = \overset{\star}{\boldsymbol{F}}{}_0^{(geom)} + \tilde{\boldsymbol{F}}_0^{(geom)}. \tag{8.7}$$

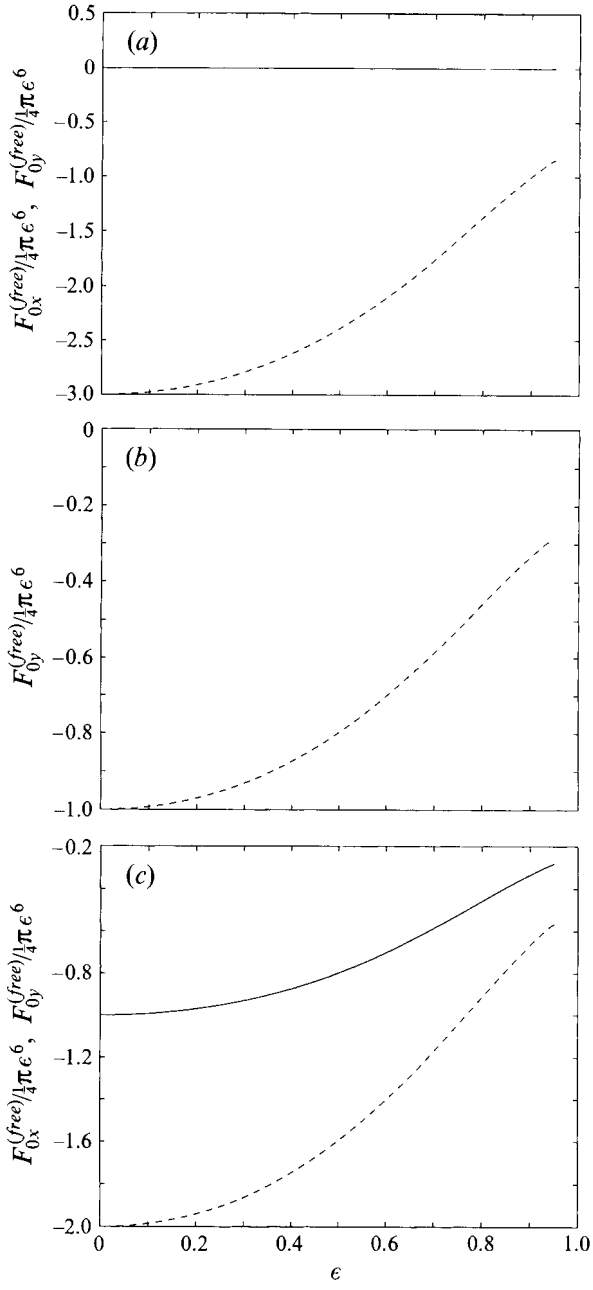

FIGURE 10. Force components $F_{0x}^{(free)}$ (solid curves) and $F_{0y}^{(free)}$ (dashed curves) divided by $(\pi\epsilon^6/4)$ and given as functions of the radius ϵ. The exact Fourier series (8.6) is truncated to 20 terms in both n and m. (*a*) Vertical motion ($\alpha = \frac{1}{2}\pi$). (*b*) Horizontal motion ($\alpha = 0$). (*c*) Oblique motion ($\alpha = \frac{1}{4}\pi$).

These are defined by means of the potentials $\overset{\star}{\psi}_1$ and $\tilde{\psi}_1$ derived in Appendix B:

$$\overset{\star}{\boldsymbol{F}}_0^{(geom)} = \epsilon \int_{-\pi}^{\pi} \overset{\star}{\psi}_1(\epsilon, \Theta)\, \boldsymbol{i}_R \, \mathrm{d}\Theta, \quad \tilde{\boldsymbol{F}}_0^{(geom)} = \epsilon \int_{-\pi}^{\pi} \tilde{\psi}_1(\epsilon, \Theta)\, \boldsymbol{i}_R \, \mathrm{d}\Theta. \qquad (8.8\,a, b)$$

The first of these can be rewritten in bipolar coordinates as

$$\overset{\star}{F}{}_0^{(geom)} = -4\tanh\zeta_0 \sum_{n=1}^{\infty}\sum_{m=1}^{\infty}(-1)^{n+m}nm\,\mathrm{e}^{-(n+m)\zeta_0}$$
$$\times\Big[\boldsymbol{i}\sin\alpha\int_{-\pi}^{\pi}((1+\cosh\zeta_0\cos\theta)\sin(n\theta+\alpha)$$
$$+\sinh\zeta_0\sin\theta\cos(n\theta+\alpha)\tanh\zeta_0)\sin m\theta\,\mathrm{d}\theta$$
$$+\boldsymbol{j}\cos\alpha\int_{-\pi}^{\pi}(\sinh\zeta_0\sin\theta\sin(n\theta+\alpha)$$
$$-(1+\cosh\zeta_0\cos\theta)\cos(n\theta+\alpha)\tanh n\zeta_0)\cos m\theta\,\mathrm{d}\theta\Big]. \tag{8.9}$$

Here the Fourier expansions (A 2) and (A 3) have been used. Carrying out the integration finally leads to the formula

$$\overset{\star}{F}{}_0^{(geom)} = -4\pi\tanh\zeta_0\sinh\zeta_0\cos\alpha\,(\boldsymbol{i}\sin\alpha+\boldsymbol{j}\cos\alpha)$$
$$\times\sum_{n=1}^{\infty}n\,\mathrm{e}^{-2n\zeta_0}(\tanh n\zeta_0-1)(n\sinh\zeta_0-\cosh\zeta_0). \tag{8.10}$$

This force contribution makes an angle with the velocity $\boldsymbol{R}_1$ (i.e. gives a lift component) except in the cases $\alpha=\frac{1}{4}\pi$ and $\alpha=\frac{1}{2}\pi$. The second force contribution is found to be

$$\tilde{\boldsymbol{F}}_0^{(geom)} = -2\pi\sin\alpha\,\boldsymbol{R}_1\tanh\zeta_0\sum_{n=1}^{\infty}\frac{n\,\mathrm{e}^{-2n\zeta_0}}{\cosh n\zeta_0}$$
$$\times\left[\frac{(n-1)\,\mathrm{e}^{\zeta_0}}{\cosh(n-1)\zeta_0}-2\frac{n}{\cosh n\zeta_0}+\frac{(n+1)\,\mathrm{e}^{-\zeta_0}}{\cosh(n+1)\zeta_0}\right]. \tag{8.11}$$

Equations (8.10)–(8.11) are summed to obtain the zeroth-order force due to geometric nonlinearity (8.7). In figure 11 we show the force components $F_{0x}^{(geom)}$ (solid curves) and $F_{0y}^{(geom)}$ (dashed curves) as functions of the cylinder radius ϵ for vertical, horizontal and oblique motion ($\alpha=\frac{1}{2}\pi,\ 0,\ \frac{1}{4}\pi$). In the diagrams these force components have been divided by $(\frac{1}{2}\pi\epsilon^4)$, in order to allow a direct comparison with (8.4). It was hoped that this asymptotic formula (derived by Tyvand & Miloh 1995) would be valid in the small-cylinder limit. But the comparisons of these curves with (8.4) fail, even though it is confirmed that the force components are of order ϵ^4 when ϵ is small.

However, we have performed a separate comparison of (8.11) with (8.4), and found very good agreement (less than 1% deviation) when $\epsilon<0.1$. This leads us to the conclusion that the contribution (8.11) is consistent with our small-cylinder assumption of locally uniform flow. On the other hand, the contribution (8.10) is incompatible with our small-cylinder approximation, no matter how small the cylinder is. So there are two qualitatively different force effects due to geometric nonlinearity. (i) The first, obvious effect is that the cylinder carries the (modified) initial flow field with it into a new location. This is the field given by zero-potential condition at the free surface and by the forced motion at the cylinder contour. It makes a small cylinder behave like a

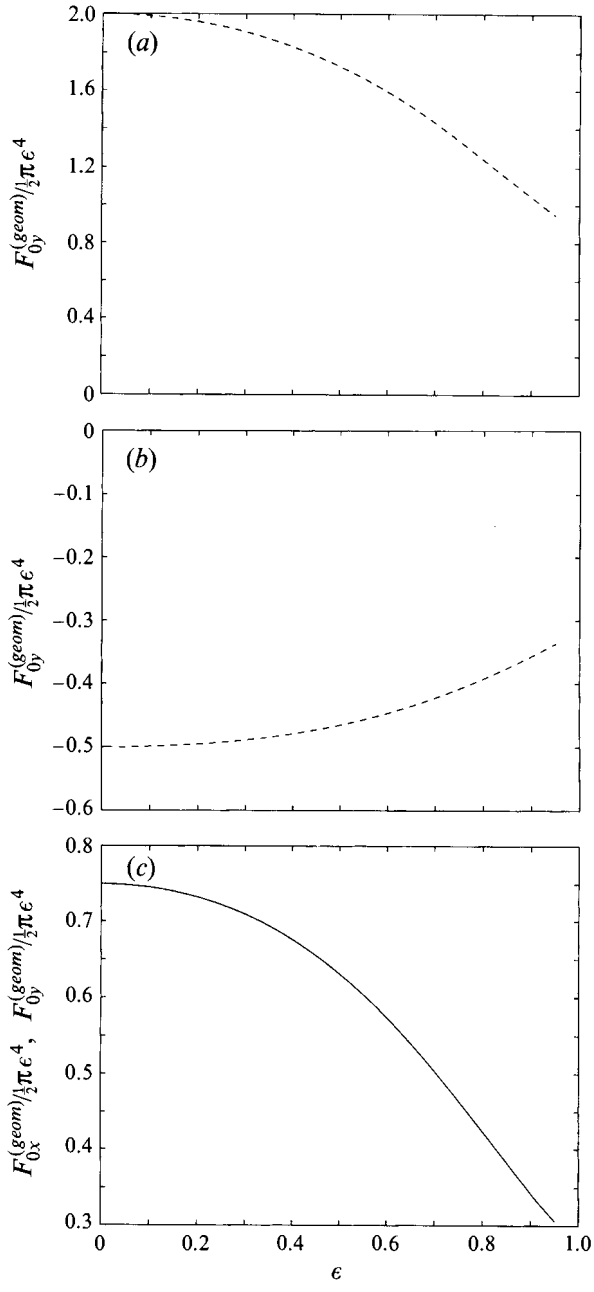

FIGURE 11. Force components $F_{0x}^{(geom)}$ (solid curves) and $F_{0y}^{(geom)}$ (dashed curves) divided by $(\pi\epsilon^4/2)$ and given as functions of the radius ϵ. The exact Fourier series (8.10) and (8.11) are truncated to 20 terms. (*a*) Vertical motion ($\alpha = \frac{1}{2}\pi$). (*b*) Horizontal motion ($\alpha = 0$). (*c*) Oblique motion ($\alpha = \frac{1}{4}\pi$).

dipole in a uniform flow. Its force is given by (8.11). (ii) The second (less obvious) effect is that the cylinder penetrates a finite distance into the initial field (that it has been continuously producing since time zero, to generate the first-order elevation). With our small-time extrapolation from time zero, the initial field continues to operate, even after the cylinder has moved a finite distance away from its initial location. The force

due to this interaction between the initial field and the displaced cylinder is represented by (8.10). This cannot be captured in our small-cylinder limit. But we note that (8.10) is zero for vertical motion: this is the only case where the inconsistency of the small-cylinder theory is due entirely to the dynamic-pressure force (8.5).

The horizontal force $F_{0x}^{(geom)}$ exists only when the motion is oblique. Usually this horizontal force is smaller than the corresponding vertical force. But in our displayed case $\alpha = \frac{1}{4}\pi$ the horizontal and vertical forces due to geometric nonlinearity are exactly equal.

Generally all zeroth-order force components have magnitudes increasing monotonically with the cylinder radius. The vertical forces are usually more important then the horizontal forces, which exist only when the motion is oblique. We note that the vertical force due to geometric nonlinearity is positive when the motion is vertical ($\alpha = \frac{1}{2}\pi$), while it is negative in the two other displayed cases ($\alpha = 0, \frac{1}{4}\pi$).

Through our choice of dimensionless quantities, all zeroth-order forces are proportional to the square of the cylinder velocity. The net zeroth-order force will always point upwards when the cylinder moves vertically. Generally the zeroth-order force is conserved under a reversal of the direction of motion:

$$\boldsymbol{F}_0(\alpha+\pi) = \boldsymbol{F}_0(\alpha). \tag{8.12}$$

These conclusions concerning the direction and magnitude of the zeroth-order force agree with those stated by Greenhow (1988). However, his analysis is rather crude, and it is restricted to vertical motion only. When the cylinder moves horizontally, there will be a net downward zeroth-order force (negative lift).

9. The leading-order gravitational effects

In the case of a constant velocity, the leading gravitational effects enter into our perturbation scheme through the second-order potential. From (3.10) the free-surface condition for the leading-order gravitational contribution to the potential is

$$\Phi_2^{(Fr)} = -\frac{\eta_1}{2Fr^2}, \quad y = 0. \tag{9.1}$$

In addition we have the condition (3.21*b*) of zero normal derivative at the cylinder contour. From formula (5.7) it is now straightforward to find the leading-order gravity-dependent potential:

$$\Phi_2^{(Fr)} = \frac{1}{2Fr^2}\sum_{n=1}^{\infty}\frac{(-1)^n n\,\mathrm{e}^{-n\zeta_0}}{\cosh n\zeta_0}\left[\frac{\sin((n-1)\theta+\alpha)\cosh(n-1)(\zeta-\zeta_0)}{\cosh(n-1)\zeta_0}\right.$$
$$\left.+2\frac{\sin(n\theta+\alpha)\cosh n(\zeta-\zeta_0)}{\cosh n\zeta_0}+\frac{\sin((n+1)\theta+\alpha)\cosh(n+1)(\zeta-\zeta_0)}{\cosh(n+1)\zeta_0}\right]. \tag{9.2}$$

From the kinematic condition (3.14) we can now determine the leading-order gravitational effect on the surface elevation:

$$\eta_3^{(Fr)} = -\frac{1}{3h_\zeta}\frac{\partial\Phi_2^{(Fr)}}{\partial\zeta}(0,\theta)$$
$$= \frac{\cos^2(\frac{1}{2}\theta)}{3\,Fr^2\tanh\zeta_0}\sum_{n=1}^{\infty}\frac{(-1)^n n\,\mathrm{e}^{-n\zeta_0}}{\cosh n\zeta_0}[(n-1)\sin((n-1)\theta+\alpha)\tanh(n-1)\zeta_0$$
$$+2n\sin(n\theta+\alpha)\tanh n\zeta_0+(n+1)\sin((n+1)\theta+\alpha)\tanh(n+1)\zeta_0]. \tag{9.3}$$

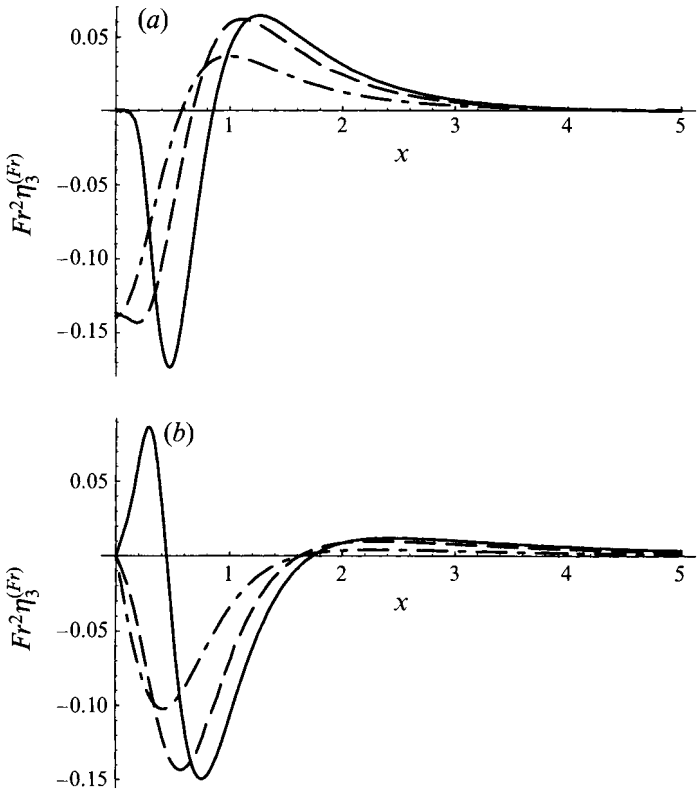

FIGURE 12. Third-order surface elevation due to gravitational effects, for three choices of dimensionless radius: $\epsilon = 0.5$ (dash-dot curves, smallest amplitude), $\epsilon = 0.8$ (dashed curves, medium amplitude), $\epsilon = 0.98$ (solid curves, largest amplitude). (*a*) Vertical motion ($\alpha = \frac{1}{2}\pi$). (*b*) Horizontal motion ($\alpha = 0$).

Figure 12 shows a plot of $(Fr^2\,\eta_3^{(Fr)})$ as a function of x for the same choices of radii as in figure 4: $\epsilon = 0.5$, 0.8 and 0.98. The exact Fourier series solution (9.3) is truncated to 40 terms. Figure 12(*a*) represents a vertical motion ($\alpha = \frac{1}{2}\pi$). When $\epsilon < 0.8$ the behaviour is as expected: there is a trough around $x = 0$, representing a radiation of wave energy out from the bulk of the first-order surface heap. Since this third-order elevation tends rather quickly to zero in the far field, there must be a positive surface elevation near $x = 1$, so as to satisfy the condition (3.28) of mass conservation. When the radius ϵ exceeds 0.8, a new feature emerges: the minimum surface elevation is displaced out from $x = 0$, where a local maximum tends to build up, although with a negative surface elevation. In order to further understand this, we consider values of ϵ close to 1, where there is a dynamically passive layer of fluid around $x = 0$. This layer is passive because it is almost at rest relative to the cylinder, following its forced upward motion with the unit velocity. In this passive layer there will be no gravitational effects at small times, as is clearly seen in the case $\epsilon = 0.98$ in figure 12(*a*). The local maximum emerging at $x = 0$ as ϵ exceeds 0.8 can thus be interpreted as the beginning transition to this passive layer configuration. In all three cases displayed, the third-order minimum is located near the point where the first-order surface slope reaches a maximum. So the leading-order gravitational effect may possibly reduce the tendency of surface breaking.

Figure 12(*b*) represents the case of horizontal motion ($\alpha = 0$). Here this third-order

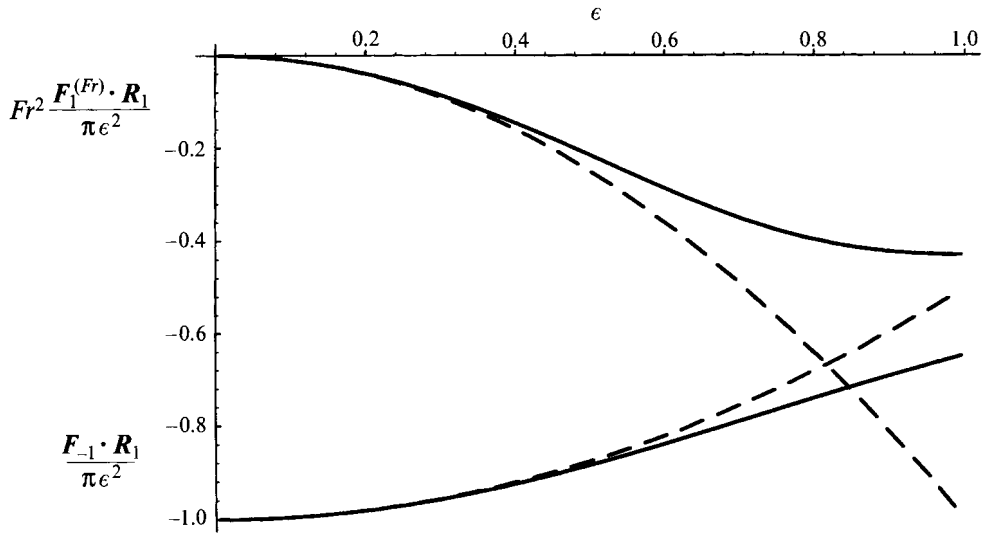

FIGURE 13. Gravitational hydrodynamic force $F_1^{(Fr)} \cdot R_1$, multiplied by Fr^2 and divided by the displaced fluid mass $\pi\epsilon^2$ (upper curves). Lower curves represent the initial impulsive force divided by displaced fluid mass. The curves are functions of the dimensionless radius ϵ. Solid curves: exact Fourier series solutions (9.4) and (6.5), truncated to 100 terms. Dashed curves: leading-order small-cylinder approximations (6.6) to order ϵ^2 and (9.6).

elevation is antisymmetric, so there is no need for a surface crest (for $x > 0$) to assure mass conservation. Also in this case, the behaviour for $\epsilon < 0.8$ is as expected: there is a surface trough located near the first-order crest, representing outward radiation of wave energy. However, when $\epsilon > 0.83$, a positive surface crest emerges near the origin. The physical explanation is far from being clear, but it may possibly be related to the occurrence of the maximal first-order slope. When $\epsilon > 0.83$ the third-order elevation tends to increase the maximal slope, so there is a possibility that gravity enhances surface breaking.

We will also calculate the leading-order gravitational force from the fluid on the cylinder, which grows linearly in time. It is given by

$$\begin{aligned} \boldsymbol{F}_1^{(Fr)} &= 2\epsilon \int_{-\pi}^{\pi} \phi_2^{(Fr)}(\epsilon, \Theta)\, \boldsymbol{i}_R \, \mathrm{d}\Theta \\ &= 2\tanh\zeta_0 \int_{-\pi}^{\pi} \Phi_2^{(Fr)}(\zeta_0, \theta) \frac{i\sinh\zeta_0 \sin\theta + j(1+\cosh\zeta_0\cos\theta)}{(\cosh\zeta_0 + \cos\theta)^2} \mathrm{d}\theta. \end{aligned} \tag{9.4}$$

Here we have performed a transformation from polar coordinates to bipolar coordinates, and introduced Cartesian unit vectors. By inserting the potential (9.2) and the Fourier expansions (A 2) and (A 3), we finally obtain the formula

$$\boldsymbol{F}_1^{(Fr)} = 2\pi Fr^{-2} \boldsymbol{R}_1 \tanh\zeta_0 \sum_{n=1}^{\infty} \frac{n\mathrm{e}^{-2n\zeta_0}}{\cosh n\zeta_0} \left[\frac{(n-1)\mathrm{e}^{\zeta_0}}{\cosh(n-1)\zeta_0} - 2\frac{n}{\cosh n\zeta_0} + \frac{(n+1)\mathrm{e}^{-\zeta_0}}{\cosh(n+1)\zeta_0} \right]. \tag{9.5}$$

This leading-order gravitational force points in the direction opposite to the initial velocity. In figure 13 we show this first-order gravitational force divided by the infinite-fluid added mass ($\pi\epsilon^2$), as a function of the radius ϵ (lower solid curve). It is compared with a dashed curve representing the asymptotic formula (Tyvand & Miloh 1995, equation (5.13)) which is valid as $\epsilon \to 0$:

$$\boldsymbol{F}_1^{(Fr)}/(\pi\epsilon^2) = -(\epsilon^2/Fr^2)\boldsymbol{R}_1. \tag{9.6}$$

For comparison we also redraw the initial impulse force from figure 5, (6.5). This is the lower curve in figure 13, with the accompanying dashed curve representing two terms in the asymptotic expansion (6.6). The series expansions have been truncated to 100 terms.

When ϵ is of order 0.5 or smaller, the agreement with the one-term asymptotic formulae is acceptable and about the same in both cases displayed in figure 13. But there is an interesting difference between the two cases for larger ϵ: the tangent of the curve for the first-order force becomes horizontal as $\epsilon \to 1$, whereas the curve for the added momentum approaches $\epsilon = 1$ with a finite slope. An explanation is that the thin, gravitationally passive layer above a cylinder with radius close to 1 does not contribute to the added mass in the gravity-dependent second-order flow. At zeroth order, however, this layer has a large velocity (close to 1 for purely vertical motion), so it does contribute to the added mass with the zeroth-order flow.

The leading gravitational effects on the surface elevation as well as the hydrodynamic force are specified by linear theory. So the principle of superposition is valid for the gravitational surface elevation and force when the cylinder performs an oblique motion. We display no results for oblique motion, since they are given by linear combinations of horizontal and vertical motion.

10. The case of a constant acceleration from rest

In our above exact theory (§§5–9) we have taken $X_2 = Y_2 = 0$, thus assuming that the forced motion has no acceleration. In this section we will consider the opposite case, where X_2, Y_2 or both are non-zero, while there is no initial velocity:

$$\hat{\boldsymbol{R}}_1 = 0. \tag{10.1}$$

We will try to deduce the results for a cylinder in constant acceleration from the above analysis with constant speed. In order to clarify the necessary transformations we have introduced the superscript $\hat{}$ for the case of constant acceleration, whereas the case of constant speed will be left without any superscript.

Redefining α as the angle (measured counter-clockwise) between the initial acceleration vector and the x-axis, the dimensionless acceleration of the cylinder is defined as

$$\frac{\mathrm{d}^2\hat{\boldsymbol{R}}}{\mathrm{d}t^2} = 2\hat{\boldsymbol{R}}_2 = \boldsymbol{i}\cos\alpha + \boldsymbol{j}\sin\alpha, \tag{10.2}$$

which is analogous to (6.4) for the case of a constant velocity. Thus, the absolute value of the dimensionless acceleration is 1 according to our definition. This means that the dimensional acceleration (A) is given by (W^2/D), i.e.

$$W = (AD)^{1/2}. \tag{10.3}$$

The Froude number (2.1) is thus defined as an acceleration ratio:

$$Fr = (A/g)^{1/2}. \tag{10.4}$$

From now on, the meaning of α will alternate between the definitions (6.4) and (10.2), i.e. α denotes in general the angle between the direction of forced motion and the x-axis. Then we may write

$$\hat{\boldsymbol{R}}_2 = \tfrac{1}{2}\boldsymbol{R}_1. \tag{10.5}$$

By comparing the boundary conditions (3.19) and (3.20) we immediately find

$$\hat{\boldsymbol{\Phi}}_1 = \boldsymbol{\Phi}_0 \tag{10.6}$$

because the first-order potential now vanishes on the free surface. From the kinematic conditions (3.12) and (3.13) we then get

$$\hat{\eta}_1 = 0, \tag{10.7}$$

$$\hat{\eta}_2 = \tfrac{1}{2}\eta_1. \tag{10.8}$$

By comparing (6.1) and (8.2*b*) we find the zeroth-order force:

$$\hat{\boldsymbol{F}}_0 = \boldsymbol{F}_{-1}. \tag{10.9}$$

This has already been displayed in figure 5, as a function of the inverse radius. In this case the added mass retains its usual link to the acceleration (instead of momentum), and it is also given by Greenhow & Li (1987, figure 2) for zero potential at the free surface.

According to conditions (3.10) and (3.21*a*) there are no inhomogeneous boundary conditions for the second-order potential, which will be zero:

$$\hat{\Phi}_2 = 0. \tag{10.10}$$

So there is no third-order elevation in the case of constant acceleration:

$$\hat{\eta}_3 = 0. \tag{10.11}$$

The leading-order effects of convective acceleration and geometric nonlinearity join the leading gravitational effect in the third-order potential:

$$\hat{\Phi}_3 = \tfrac{1}{3}(6\phi_1 + \psi_1 + \phi_2^{(Fr)}). \tag{10.12}$$

This gives the formula for the full fourth-order surface elevations:

$$\hat{\eta}_4(x) = \frac{1}{2}\frac{\partial \phi_1}{\partial y}(x,0) + \frac{1}{12}\frac{\partial \psi_1}{\partial y}(x,0) + \tfrac{1}{4}\eta_3^{(Fr)}(x). \tag{10.13}$$

Here we benefit from the splitting of the potential introduced in (3.23).

We close this section by calculating higher-order forces. It is easily shown that the first-order force vanishes:

$$\hat{\boldsymbol{F}}_1 = 0. \tag{10.14}$$

The second-order force is defined by the following integral:

$$\hat{\boldsymbol{F}}_2 = \epsilon \int_{-\pi}^{\pi} (3\hat{\Phi}_3 + \tfrac{1}{2}|\nabla \hat{\Phi}_1|^2)\, \boldsymbol{i}_R \, \mathrm{d}\Theta, \quad r = \epsilon. \tag{10.15}$$

This quantity can be expressed by force components derived in the two preceding sections:

$$\hat{\boldsymbol{F}}_2 = \boldsymbol{F}_0^{(dyn)} + 6\boldsymbol{F}_0^{(free)} + \boldsymbol{F}_0^{(geom)} + \tfrac{1}{2}\boldsymbol{F}_1^{(Fr)}. \tag{10.16}$$

We note that the free-surface nonlinearity is relatively much more important for constant acceleration than for constant speed. We also note that the leading gravitational effects with constant acceleration enter the problem to the same order as the leading nonlinear effects.

11. Summary and discussion

A small-time expansion has been performed for the unsteady nonlinear free-surface flow generated by the forced motion of a circular cylinder impulsively started from rest at time zero. The forced motion is either with constant velocity or constant

acceleration, and our expansion has been taken far enough to include the leading-order gravitational effects. The surface elevation and the hydrodynamic force are calculated to each order in the expansion.

Both the initial force impulse and the leading gravitational force are vectors pointing in a direction opposite to the motion of the cylinder. Thus reversing the direction of motion means reversing these forces. As a contrast, the steady (zeroth-order) force is unchanged when the direction of motion is reversed. The steady force is proportional to the square of the velocity, and it is purely vertical both for horizontal and vertical motion. Only in the case of oblique motion does a horizontal steady force component arise. It can be interpreted as being due to nonlinear interaction between the zeroth-order flows due to horizontal and vertical motion of the cylinder.

From the expressions for the force one may easily calculate the work exerted by the cylinder on the surrounding fluid. The work may then be given as a power series in time. We mention one obvious result: the zeroth-order work is given by the initial kinetic energy of the fluid, and is equal to the added mass times half the squared initial velocity.

Only one of the present results has been derived in the literature: the initial force impulse experienced by the cylinder during the impulsive start. It was calculated by Venkatesan (1985) and Greenhow & Li (1987). In a recent analytical work, Wu (1993) has taken into account the effects of what we call 'geometric nonlinearity' at the cylinder contour, when the cylinder performs forced oscillations. He linearized the free-surface condition. Our results confirm that the geometric nonlinearity usually dominates over the free-surface nonlinearity, especially for small cylinders. In analogy with Wu, we find that geometric nonlinearity gives rise to an important steady force, although our theory permits it to be traced for a short time only.

We find exact solutions to each order, by utilizing Fourier expansions in bipolar coordinates. As an independent check of these solutions, our accompanying paper (Tyvand & Miloh 1995) gives a comparison with the much simpler small-cylinder limit solutions based on a dipole approximation for the zeroth-order flow. There is good agreement in the surface elevation when the ratio of cylinder radius to submergence depth is 0.3 or smaller. However, two zeroth-order force contributions are beyond the reach of our small-cylinder theory: both the force due to the dynamic-pressure effect and the force due to geometric nonlinearity at the cylinder contour are inconsistent with our small-cylinder theory, which assumes uniform local flow around the cylinder. Their contributions to the zeroth-order force cannot be neglected, no matter how small the cylinder is. These inconsistencies of our small-cylinder theory (Tyvand & Miloh 1995) provoke an improved physical understanding of the present general results for the hydrodynamic force. Although our small-cylinder assumption of uniform flow surrounding the cylinder is not consistent with respect to the zeroth-order force, it works for the singular impulsive force and for the first-order gravitational force.

Haussling & Coleman (1979) and Telste (1987) have studied a hybrid problem, where the cylinder is first accelerated and later kept at constant velocity. Only the stage of acceleration can be compared with our analytical theory. Figure 16 by Telste (1987) revealed an early quadratic growth with time for the surface elevation just above a cylinder (accelerated vertically). Moreover, the early gravitational effect on the elevation was the fourth power of time. Both these results support our present theory qualitatively (§10), but Telste (1987) did not give enough documentation to provide a full quantitative comparison.

A striking effect has been identified for the surface elevation of a cylinder in vertical motion close to the free surface: the surface above the cylinder will often attain an

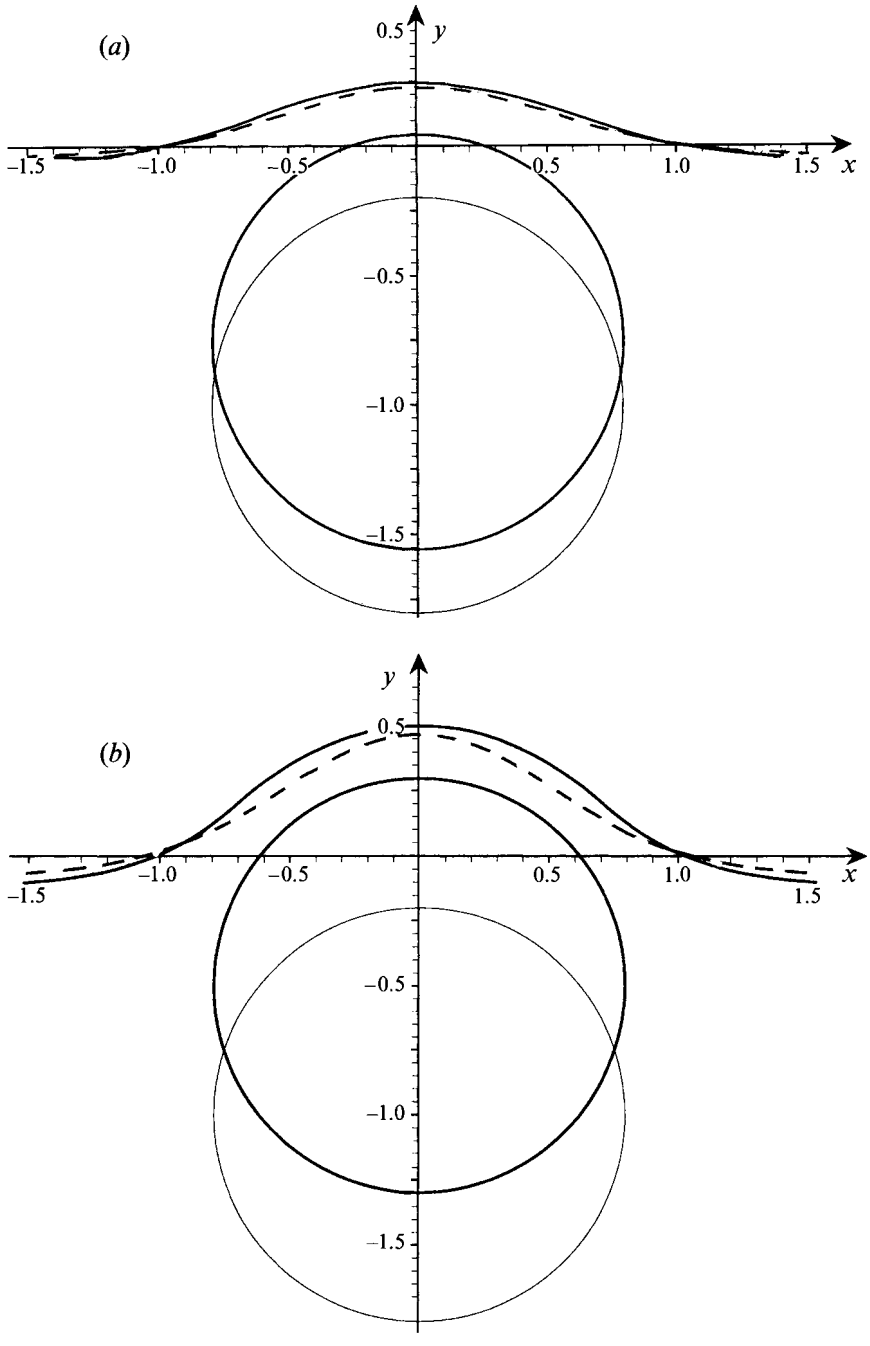

FIGURE 14(*a*,*b*). For caption see p. 97.

almost circular shape, according to the numerical simulations by Telste (1987), Greenhow (1988) and Terent'ev (1991), as well as the experiments by Greenhow & Lin (1983). When the Froude number is large, this surface shape will have its centre almost in the (instantaneous) cylinder centre, so that the radial thickness of the fluid layer above the cylinder will be almost uniform.

We are able to identify this trend of almost uniform radial thickness of the fluid layer

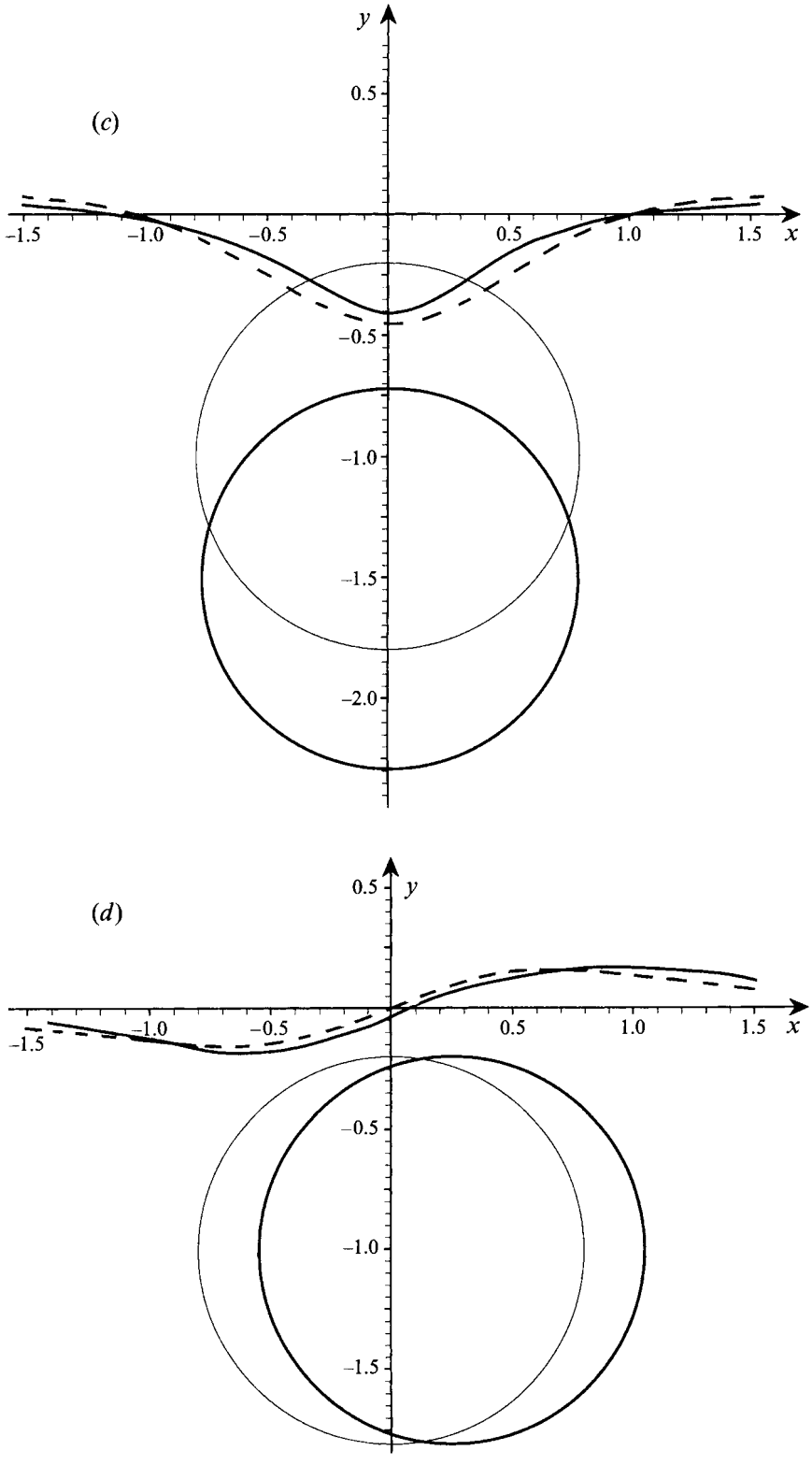

FIGURE 14(*c*,*d*). For caption see p. 97.

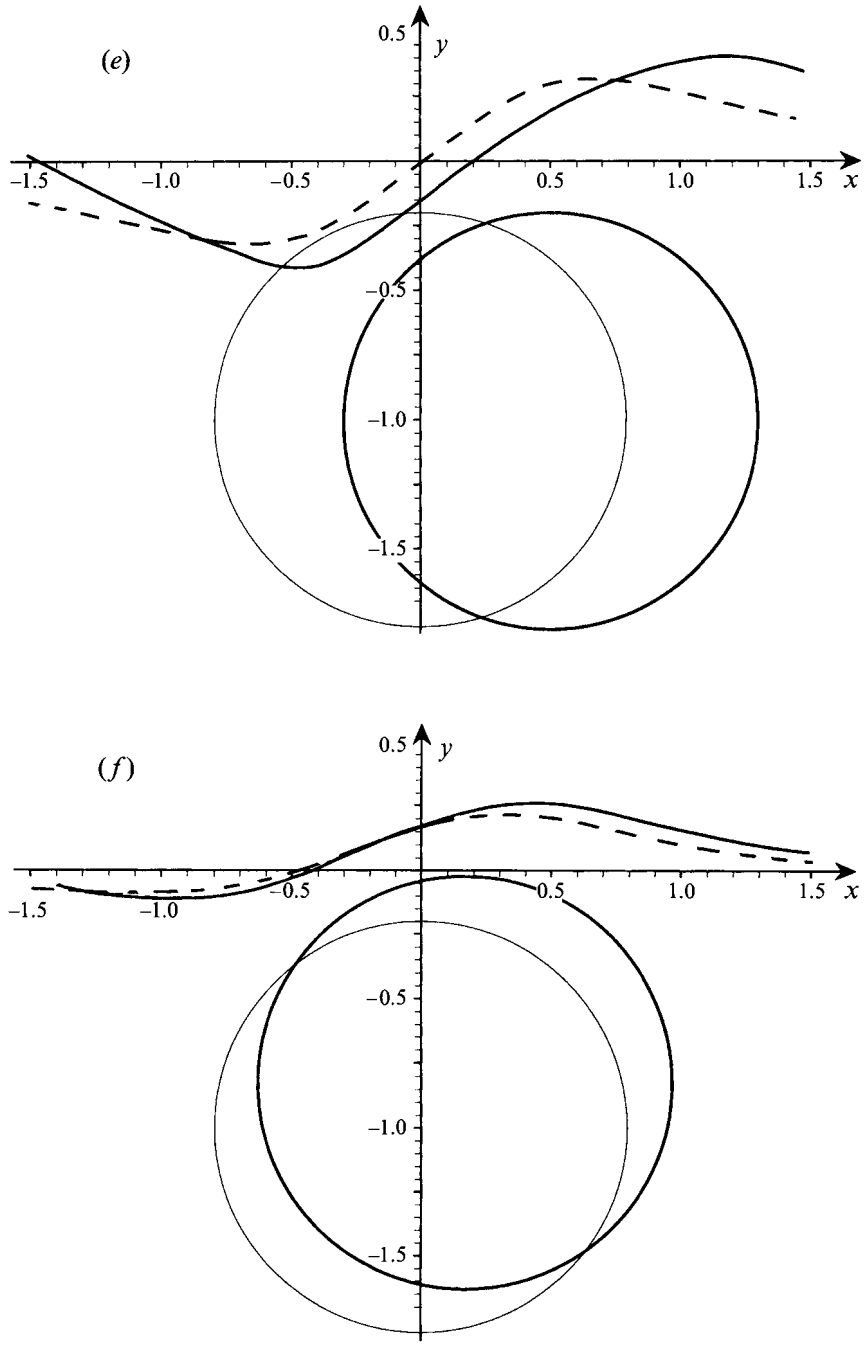

FIGURE 14(*e*,*f*). For caption see facing page.

above a large cylinder in rapid upward motion (infinite Froude number). In figure 14 we consider the cylinder radius $\epsilon = 0.8$ and display the full surface elevation (according to second-order theory) above the cylinder at dimensionless times $t = 0.25$ and 0.5. The latter value is t is as large as we can possibly allow with neglect of terms of third and higher orders, but it is useful in order to show clearly the nonlinear effects. Figure 14(*a*, *b*) shows the case of upward motion. We note that the second-order elevation

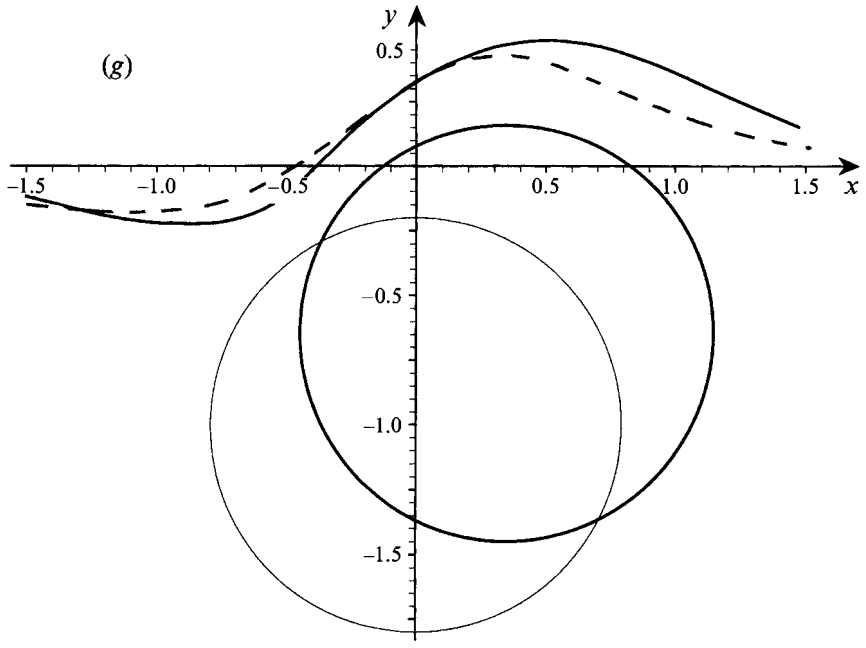

FIGURE 14. Snapshots of free surface above a large cylinder ($\epsilon = 0.8$) in rapid motion with constant speed. Solid curves: total surface elevation according to second-order theory ($\eta(x,t) = \eta_1 t + \eta_2 t^2$). Dashed curves: surface elevation according to first-order theory. Thick solid circle shows current position and thin circle shows initial position of the cylinder contour. Upward motion ($\alpha = \frac{1}{2}\pi$): (*a*) $t = 0.25$, (*b*) $t = 0.5$. Downward motion ($\alpha = -\frac{1}{2}\pi$): (*c*) $t = 0.5$. Horizontal motion ($\alpha = 0$): (*d*) $t = 0.25$, (*e*) $t = 0.5$. Oblique motion ($\alpha = \frac{1}{4}\pi$): (*f*) $t = 0.25$, (*g*) $t = 0.5$.

plays a very important role in generating the constant radial thickness, and it shifts the inflection point of the free surface to larger values of $|x|$. Figure 14(*b*) confirms the observed tendency of constant radial thickness and identifies it as a nonlinear phenomenon. Our theory cannot here be compared quantitatively with published numerical results, because all displayed simulations refer to times greater than one, where our theory is not reliable.

Figure 14(*c*) shows that a relatively narrow trough will evolve above a cylinder in forced downward motion. Figure 14(*d–g*) shows similar snapshots of the free surface for horizontal and oblique motion. Greenhow (1993, figure 5) shows a case of horizontal motion that can be compared with our theory at small times (with $\epsilon = 0.5$), and the agreement is reasonable.

A complementary way to define the present problem is to prescribe the net force on the cylinder as a function of time, and compute its resulting motion and the surface elevation. The solution of such a problem can be achieved from a reinterpretation of the present results. For example, let us assume that the cylinder is suddenly put into motion by an initial impulsive 'kick', and is afterwards left to move freely (assuming neutral buoyancy).

(i) If the cylinder is given an upward motion, it will of course continue to move upwards, but it will experience three vertical zeroth-order forces: a downward dynamic-pressure force, a downward force due to free-surface nonlinearity, and an upward force due to geometric nonlinearity. The net zeroth-order force always points upwards. Thus a cylinder of small or moderate size will get an early acceleration upwards, until gravity comes into play and retards the upward motion.

(ii) If the cylinder is given a horizontal motion, it will continue to move freely with constant speed horizontally, until gravity comes into play and retards its horizontal motion. However, the cylinder will be accelerated downwards by the zeroth-order force. Thus the early path of the cylinder is in this case a parabola, starting out horizontally and curving downwards.

E. E. Leirgul is acknowledged for drawing figures 1–3 and 14. The referees are thanked for valuable comments.

Appendix A. Fourier expansion of the zeroth-order potential

In order to find the exact solution for the zeroth-order potential, we need the Fourier expansion of the following factor (Morse & Feshbach 1953, p. 1215):

$$\frac{\sinh\zeta_0}{\cosh\zeta_0+\cos\theta} = 1+2\sum_{n=1}^{\infty}(-1)^n\,\mathrm{e}^{-n\zeta_0}\cos n\theta. \tag{A 1}$$

This formula requires ζ_0 positive, which is always true in this paper. By taking the derivative with respect to θ we get

$$\frac{\sinh\zeta_0\sin\theta}{(\cosh\zeta_0+\cos\theta)^2} = 2\sum_{n=1}^{\infty}(-1)^{n+1}n\,\mathrm{e}^{-n\zeta_0}\sin n\theta. \tag{A 2}$$

The derivative of (A 1) with respect to ζ_0 gives

$$\frac{1+\cos\theta\cosh\zeta_0}{(\cosh\zeta_0+\cos\theta)^2} = 2\sum_{n=1}^{\infty}(-1)^{n+1}n\,\mathrm{e}^{-n\zeta_0}\cos n\theta. \tag{A 3}$$

The Fourier expansion of the boundary condition at the cylinder can then be written as

$$\frac{\partial\Phi_0}{\partial\zeta}(\zeta_0,\theta) = 2\sin\alpha\tanh\zeta_0\sum_{n=1}^{\infty}(-1)^n n\,\mathrm{e}^{-n\zeta_0}\cos n\theta + 2\cos\alpha\tanh\zeta_0\sum_{n=1}^{\infty}(-1)^n n\,\mathrm{e}^{-n\zeta_0}\sin n\theta. \tag{A 4}$$

Appendix B. The boundary-value problem for the first-order potential

The first-order potential is decomposed into two components:

$$\Phi_1 = \phi_1+\psi_1. \tag{B 1}$$

The first term is generated by the inhomogeneity at the free surface (due to the convective acceleration) with a zero normal derivative at the cylinder contour. The second term is generated by the inhomogeneity at the cylinder contour (geometric nonlinearity), with a homogenous condition at the free surface.

Let us first Fourier expand the inhomogeneous boundary conditions. From (3.9) and (5.5) we get

$$\phi_1(0,\theta) = \frac{1}{16}\sum_{n=1}^{\infty}\sum_{m=1}^{\infty}(-1)^{n+m}nm\,\mathrm{e}^{-(n+m)\zeta_0}\operatorname{sech}n\zeta_0\operatorname{sech}m\zeta_0 \times\sum_{k=-2}^{2}(24-9k^2+k^4)\sum_{q=-1}^{1}q\cos((n+qm+k)\theta+(q+1)\alpha). \tag{B 2}$$

The condition (3.20) in polar coordinates is (when $X_2 = Y_2 = 0$)

$$\frac{\partial \psi_1}{\partial R}(\epsilon, \Theta) = -\frac{\partial}{\partial R}(\boldsymbol{R}_1 \cdot \nabla \Phi_0), \quad R = \epsilon. \tag{B 3}$$

By definition, we have the homogeneous boundary conditions (written in bipolar coordinates):

$$\frac{\partial \phi_1}{\partial \zeta}(\zeta_0, \theta) = 0, \tag{B 4}$$

$$\psi_1(0, \theta) = 0. \tag{B 5}$$

the harmonic function that satisfies the boundary conditions (B 2) and (B 4) as well as the far-field condition (3.5) is given by

$$\phi_1(\zeta, \theta) = \frac{1}{16} \sum_{n=1}^{\infty} \sum_{m=1}^{\infty} (-1)^{n+m} nm \, \mathrm{e}^{-(n+m)\zeta_0} \operatorname{sech} n\zeta_0 \operatorname{sech} m\zeta_0 \sum_{k=-2}^{2} (24 - 9k^2 + k^4)$$
$$\times \sum_{q=-1}^{1} q \cos((n+qm+k)\theta + (q+1)\alpha) \frac{\cosh(n+qm+k)(\zeta - \zeta_0)}{\cosh(n+qm+k)\zeta_0}. \tag{B 6}$$

It proves convenient to split the function ψ_1 further into two contributions:

$$\psi_1 = \overset{\star}{\psi}_1 + \tilde{\psi}_1. \tag{B 7}$$

A qualitative definition of these functions is that the first one takes care of the inhomogeneous condition at the cylinder contour, while the second one takes care of the zero-potential condition at the free surface. Precisely, we pick the first function by formally integrating the boundary condition (B 3) in the normal (radial) direction:

$$\overset{\star}{\psi}_1(R, \Theta) = -\boldsymbol{R}_1 \cdot \nabla \Phi_0(R, \Theta). \tag{B 8}$$

This may be perceived as an analytic continuation over the fluid domain of an inhomogeneity that is only defined at the boundary. It is not a recommended procedure for solving a boundary-value problem, but makes sense here because Laplace's equation and the far-field condition are satisfied. The second function is now determined by the free-surface condition:

$$\tilde{\psi}_1(y = 0) = -\overset{\star}{\psi}_1(y = 0) = \eta_1 \sin\alpha. \tag{B 9}$$

This second function obeys zero normal derivative at the cylinder contour:

$$\frac{\partial \tilde{\psi}_1}{\partial R}(\epsilon, \Theta) = 0. \tag{B 10}$$

The first function is known already from (B 8):

$$\overset{\star}{\psi}_1(R, \Theta) = -\sin(\Theta + \alpha) \frac{\partial \Phi_0}{\partial R} - \frac{\cos(\Theta + \alpha)}{R} \frac{\partial \Phi_0}{\partial \Theta}. \tag{B 11}$$

Here we will introduce bipolar coordinates only as far as they are needed to perform the differentiations of the Fourier series (5.4):

$$\overset{\star}{\psi}_1(\zeta,\theta) = \sin(\Theta+\alpha)\,h_\zeta^{-1}\frac{\partial \Phi_0}{\partial \zeta} - \frac{\cos(\Theta+\alpha)}{R}\frac{\partial \Phi_0}{\partial \theta}\frac{\mathrm{d}\theta}{\mathrm{d}\Theta}$$

$$= 2\sum_{n=1}^{\infty}\frac{(-1)^n n\,\mathrm{e}^{-n\zeta_0}}{\cosh n\zeta_0}[\sin(\Theta+\alpha)(\cosh\zeta+\cos\theta)\sin(n\theta+\alpha)\cosh n\zeta$$

$$-(\mathrm{d}\theta/\mathrm{d}\Theta)\tanh\zeta_0\,R^{-1}\cos(\Theta+\alpha)\cos(n\theta+\alpha)\sinh n\zeta]. \qquad \text{(B 12)}$$

In the main text this formula will be applied only to a force calculation. We then need the value of this first function at the cylinder contour only:

$$\overset{\star}{\psi}_1(\zeta_0,\theta) = 2\sum_{n=1}^{\infty}(-1)^n n\,\mathrm{e}^{-n\zeta_0}$$

$$\times[\sin(\Theta+\alpha)(\cosh\zeta_0+\cos\theta)\sin(n\theta+\alpha)$$

$$-(\sin\theta/\sin\Theta)\sinh\zeta_0\cos(\Theta+\alpha)\cos(n\theta+\alpha)\tanh n\zeta_0]. \qquad \text{(B 13)}$$

At this stage we eliminate the angle Θ by (4.9) and get

$$\overset{\star}{\psi}_1(\zeta_0,\theta) = 2\sum_{n=1}^{\infty}(-1)^n n\,\mathrm{e}^{-n\zeta_0}$$

$$\times[(\sinh\zeta_0\sin\theta\cos\alpha+(1+\cosh\zeta_0\cos\theta)\sin\alpha)\sin(n\theta+\alpha)$$

$$+(\sinh\zeta_0\sin\theta\sin\alpha-(1+\cosh\zeta_0\cos\theta)\cos\alpha)\cos(n\theta+\alpha)\tanh n\zeta_0]. \qquad \text{(B 14)}$$

The second function is proportional to the second-order gravity-dependent potential (9.2), derived in the main text:

$$\tilde{\psi}_1(\zeta,\theta) = -\sin\alpha\sum_{n=1}^{\infty}\frac{(-1)^n n\,\mathrm{e}^{-n\zeta_0}}{\cosh n\zeta_0}\left[\frac{\sin((n-1)\theta+\alpha)\cosh(n-1)(\zeta-\zeta_0)}{\cosh(n-1)\zeta_0}\right.$$

$$\left.+2\frac{\sin(n\theta+\alpha)\cosh n(\zeta-\zeta_0)}{\cosh n\zeta_0}+\frac{\sin((n+1)\theta+\alpha)\cosh(n+1)(\zeta-\zeta_0)}{\cosh(n+1)\zeta_0}\right]. \qquad \text{(B 15)}$$

REFERENCES

ANANTHAKRISHNAN, P. & YEUNG, R. W. 1994 Free-surface and submerged-body interactions in a viscous fluid. *12th US Natl Congr. of Applied Mechanics, Seattle, Washington.*

BATCHELOR, G. K. 1967 *An Introduction to Fluid Dynamics.* Cambridge University Press.

DEAN, W. R. 1948 On the reflection of surface waves from a submerged circular cylinder. *Proc. Camb. Phil. Soc.* **44**, 483–491.

GREENHOW, M. 1988 Water-entry and -exit of a horizontal circular cylinder. *Appl. Ocean Res.* **10**, 191–198.

GREENHOW, M. 1993 A complex variable method for the floating-body boundary-value problem. *J. Comput. Appl. Maths* **46**, 115–128.

GREENHOW, M. & LI, Y. 1987 Added masses for circular cylinders near or penetrating fluid boundaries – review, extension and application to water-entry, -exit and slamming. *Ocean Engng* **14**, 325–348.

GREENHOW, M. & LIN, W.-M. 1983 Nonlinear free surface effects: experiments and theory. *Rep.* 83–119. MIT, Dept. of Ocean Engineering.

HAUSSLING, H. J. & COLEMAN, R. M. 1979 Nonlinear water waves generated by an accelerated circular cylinder. *J. Fluid Mech.* **92**, 767–781.

HAVELOCK, T. H. 1949*a* The wave resistance of a cylinder started from rest. *Q. J. Mech. Appl. Maths* **2**, 325–334.

HAVELOCK, T. H. 1949*b* The resistance of a submerged cylinder in accelerated motion. *Q. J. Mech. Appl. Maths* **2**, 419–427.

MILNE-THOMSON, L. M. 1968 *Theoretical Hydrodynamics*. MacMillan.

MILOH, T. 1991*a* On the initial slamming of a rigid sphere in a vertical water entry. *Appl. Ocean Res.* **13**, 43–48.

MILOH, T. 1991*b* On the oblique water-entry problem of a rigid sphere. *J. Engng Maths* **25**, 77–92.

MOON, P. & SPENCER, D. E. 1988 *Field Theory Handbook*. Springer.

MORSE, P. M. & FESHBACH, H. 1953 *Methods of Theoretical Physics*. McGraw-Hill.

OGILVIE, T. F. 1963 First- and second-order forces on a cylinder submerged under a free surface. *J. Fluid Mech.* **16**, 451–472.

PEREGRINE, D. H. 1972 Flow due to a vertical plate moving in a channel. Unpublished note.

TELSTE, J. G. 1987 Inviscid flow about a cylinder rising to a free surface. *J. Fluid Mech.* **182**, 149–168.

TERENT'EV, A. G. 1991 Nonstationary motion of bodies in a fluid. *Proc. Steklov Inst. Maths* **186**, 211–221.

TUCK, E. O. 1965 The effect of non-linearity on flow past a submerged cylinder. *J. Fluid Mech.* **22**, 401–414.

TYVAND, P. A. 1991 Motion of a vortex near a free surface. *J. Fluid Mech.* **225**, 673–686 (appendix by R. P. Tong).

TYVAND, P. A. & MILOH, T. 1995 Free-surface flow generated by a small submerged circular cylinder starting from rest. *J. Fluid Mech.* **286**, 103–116.

URSELL, F. 1950 Surface waves on deep water in the presence of a submerged circular cylinder. *Proc. Camb. Phil. Soc.* **46**, 141–158.

VENKATESAN, S. K. 1985 Added mass of two cylinders. *J. Ship Res.* **29**, 234–240.

VINJE, T. 1994 On small-time expansion of nonlinear free surface problems. *J. Engng Maths* **28**, 173–190.

WU, G. X. 1993 Hydrodynamic forces on a submerged circular cylinder undergoing large-amplitude motion. *J. Fluid Mech.* **254**, 41–58.